#### Check for updates

#### **NEUROINFLAMMATION**

# Astrocytic RIPK3 exerts protective anti-inflammatory activity in mice with viral encephalitis by transcriptional induction of serpins

Marissa Lindman<sup>1</sup>, Irving Estevez<sup>1</sup>, Eduard Marmut<sup>1</sup>, Evan M. DaPrano<sup>1</sup>, Tsui-Wen Chou<sup>1</sup>, Kimberly Newman<sup>2</sup>, Colm Atkins<sup>1</sup>, Natasha M. O'Brown<sup>1</sup>, Brian P. Daniels<sup>1</sup>\*

Flaviviruses pose a substantial threat to public health because of their ability to infect the central nervous system (CNS). Receptor-interacting protein kinase 3 (RIPK3) is a central coordinator that promotes neuroinflammation during viral infection of the CNS, a role that occurs independently of its canonical function in inducing necroptosis. Here, we used mouse genetic tools to induce astrocyte-specific deletion, overexpression, and chemogenetic activation of RIPK3 to demonstrate an anti-inflammatory function for astrocytic RIPK3. RIPK3 activation in astrocytes promoted host survival during flavivirus encephalitis by limiting immune cell recruitment to the CNS. Despite inducing a proinflammatory transcriptional program, astrocytic RIPK3 restrained neuroinflammation by increasing the abundance of the protease inhibitor SerpinA3N, which preserved blood-brain barrier integrity, reduced leukocyte infiltration, and improved survival outcomes during flavivirus encephalitis. These findings highlight a previously unappreciated role for astrocytic RIPK3 in suppressing pathologic neuroinflammation.

Copyright © 2025 The Authors, some rights reserved; exclusive licensee American Association for the Advancement of Science. No claim to original U.S. Government Works

#### INTRODUCTION

Flaviviruses pose an escalating threat to public health, driven by the expanding habitats of their arthropod vectors (1-3). Clinically important flaviviruses include West Nile virus (WNV), Zika virus (ZIKV), tick-borne encephalitis virus, and Japanese encephalitis virus, all of which can invade and infect the central nervous system (CNS) (4-7). Neuroinvasive flavivirus infections are often fatal, and survivors frequently face persistent neurological sequalae long after the resolution of infection (8-10). Thus, identifying mechanisms of neuropathogenesis and host protection during flavivirus encephalitis is essential for the development of targeted therapeutics to treat and manage neuroinvasive infection (11, 12).

After the invasion of flaviviruses into CNS tissues, neural cells mount robust immune responses that are essential for controlling viral spread (13–15). These responses are critical for cell-intrinsic restriction of viral replication and for recruiting peripheral immune cells that coordinate the eradication of infection (16, 17). However, whereas peripheral immune cell recruitment to the CNS is necessary for viral clearance, infiltrating leukocytes are also capable of driving substantial immunopathology and bystander injury of uninfected neural cells (18–20). Thus, the complex neuroimmune response to neuroinvasive viral infection must be tightly regulated to promote neuroprotection while limiting immunopathogenesis.

Previous work from our laboratory and others identified an important role for receptor interacting protein kinase-3 (RIPK3) in coordinating neuroimmune responses to flavivirus infections in the CNS (21, 22). RIPK3 is canonically associated with a form of lytic programmed cell death known as "necroptosis," although a growing body of work has now defined extensive functions for RIPK3 that occur independently of cell death (23–28). During flavivirus encephalitis, we showed that RIPK3 signaling in neurons drives a transcriptional program that includes a broad range of proinflammatory and antiviral effector genes that work to control infection without

<sup>1</sup>Department of Cell Biology and Neuroscience, Rutgers University, Piscataway, NJ 08854, USA. <sup>2</sup>Brain Health Institute, Rutgers University, Piscataway, NJ 08854, USA. \*Corresponding author. Email: b.daniels@rutgers.edu

inducing necroptosis (29–31). However, roles for RIPK3 in nonneuronal cells during neuroinvasive viral infections remain largely unexplored. Astrocytes are a highly abundant glial cell type that serve complex roles in both CNS homeostasis and disease. As integral components of the neurovascular unit, they regulate the integrity of the blood-brain barrier (BBB) and exert regulatory control over the recruitment and infiltration of leukocytes into the CNS parenchyma during neuroinflammatory disease states (32). The crucial anatomical positioning of these cells at the BBB and their central function in the regulation of neuroinflammation suggests the possibility of distinct, cell type–specific functions for RIPK3 in astrocytes during flavivirus infections.

In this study, we demonstrated unexpected protective functions for astrocytic RIPK3 signaling in restricting neuroinflammation. Contrary to its predominantly proinflammatory function in neurons (29–31), we showed that RIPK3 activation in astrocytes suppressed neuropathogenesis by limiting immune cell recruitment to the CNS during flavivirus encephalitis. Using conditional in vivo expression tools, including an inducible chemogenetic RIPK3 activation system, we showed that the RIPK3-dependent transcriptional program in astrocytes is enriched for serpins, a family of endogenous serine protease inhibitors with immunomodulatory activity. In particular, mice deficient in astrocytic Ripk3 exhibited substantial BBB disruption and enhanced leukocyte infiltration into the CNS. However, reconstitution of SerpinA3N in the CNS of acutely infected mice preserved BBB integrity, reduced CNS leukocyte infiltration, and prevented fatal outcomes during flavivirus encephalitis. These findings underscore previously unappreciated, cell type-specific functions for RIPK3 in astrocytes in promoting host protection during CNS viral infection.

#### **RESULTS**

## Astrocytic RIPK3 restricts flavivirus pathogenesis but not cell-intrinsic viral replication

To determine a potential role of RIPK3 signaling in astrocytes during CNS flavivirus infection, we generated mice with an astrocyte-specific deficiency of *Ripk3* by crossing mice in which exons 2 and 3

Downloaded from https://www.science.org on October 08, 2025

of the endogenous *Ripk3* locus are flanked by loxP sites (33) (*Ripk3*<sup>fl/fl</sup>) to a line expressing tamoxifen-inducible Cre recombinase under the control of the *Aldh1l1* promoter (*Aldh1l1* Cre/ERT2, shortened to *Aldh1l1* Cre hereafter). We have previously confirmed astrocyte-specific deletion of *Ripk3* in this crossed line (34) and reconfirmed it for the present study (fig. S1, A and B). We subjected these animals to several models of flavivirus encephalitis, including intracranial

infection with an ancestral African strain of ZIKV (ZIKV-MR766, Uganda 1947) or a contemporary Asian lineage strain (ZIKV-Fortaleza, Brazil 2015). We also used a subcutaneous infection model with a neurovirulent North American strain of WNV (WNV-WN02-Bird114, Texas 2002) (Fig. 1A). Mice lacking astrocytic RIPK3 (*Ripk3* <sup>fl/fl</sup> *Aldh111* Cre<sup>+</sup>) exhibited accelerated and enhanced mortality compared with littermate controls in all three infection models (Fig. 1, B

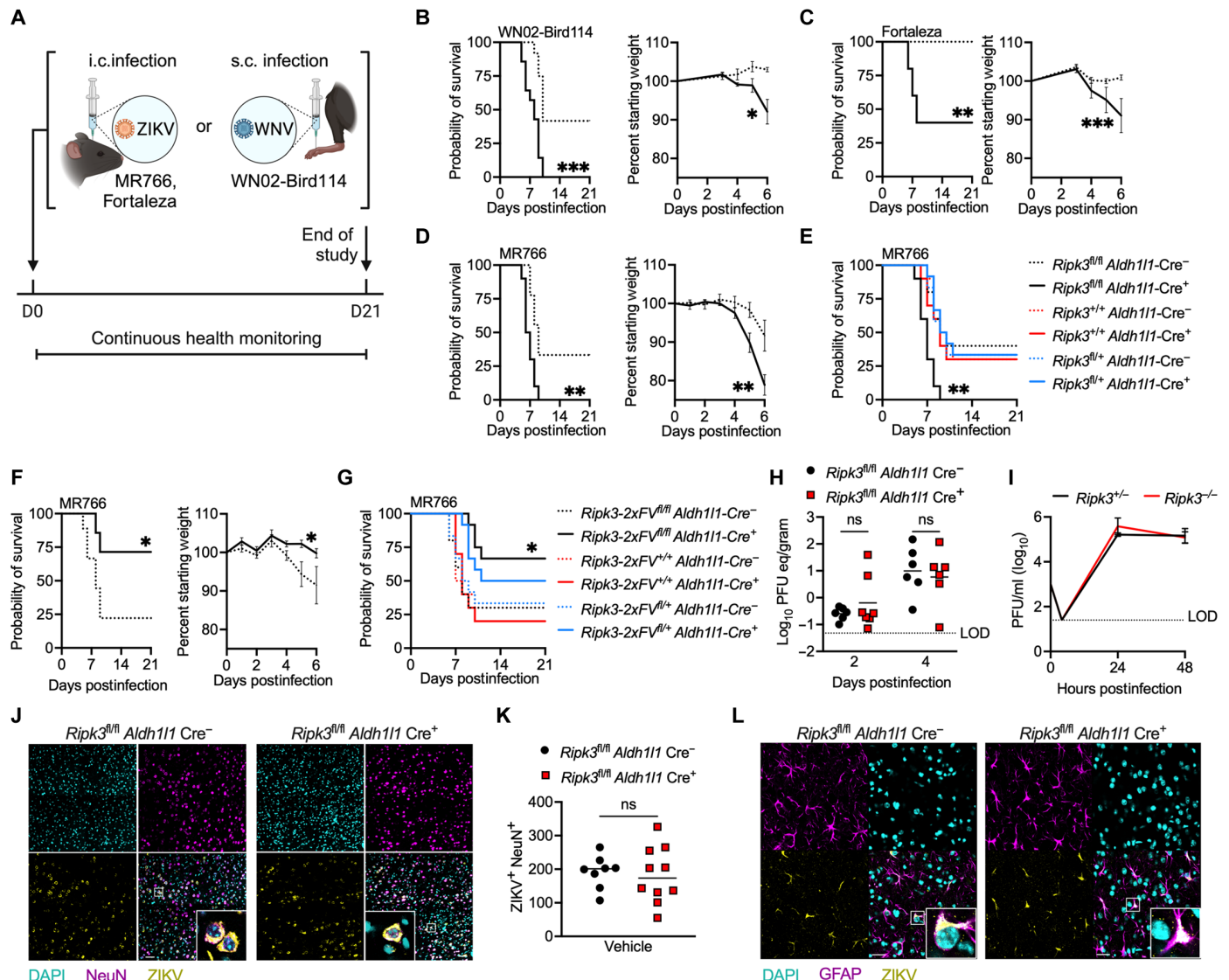


**Fig. 1. Astrocytic RIPK3 restricts flavivirus pathogenesis but not cell-intrinsic viral replication.** (**A**) Schematic illustrating survival studies in which mice underwent either intracranial (i.c.) ZIKV or subcutaneous (s.c.) WNV infections. (**B** to **G**) Survival and weight measurements in mice of the indicated genotypes after s.c. WNV-WN02-Bird114 infection [(B)], i.e. ZIKV-Fortaleza infection [(C)], or i.e. ZIKV-MR766 infection [(D) to (G)]. n = 5 to 14 mice per group. (**H**) qRT-PCR analysis of ZIKV-MR766 genome copies in whole-brain homogenates derived from mice of the indicated genotypes, 2 or 4 days after i.e. ZIKV-MR766 infection. Data are expressed as plaque-forming unit equivalents (PFU eq)/gram of brain tissue. n = 6 mice per group. LOD, limit of detection. (**I**) Multistep growth curve analysis of ZIKV-MR766 replication in primary cortical astrocytes derived from mice of the indicated genotypes. Viral titers were assessed by plaque assay. n = 4 cultures per group. (**J**) IHC staining of NeuN (magenta), DAPI (cyan), and pan–flavivirus E protein (yellow) in cortical brain tissues derived from mice of the indicated genotypes five days after i.c. ZIKV-MR766 infection. Images are  $2 \times 2$  tiled composites at  $20 \times$  magnification. Scale bar,  $20 \mu$ m. (**K**) Quantification of cells exhibiting colocalization of NeuN and pan–flavivirus E protein in cortical brain tissues derived from the mice described in (J). n = 8 to 10 mice per group. (**L**) IHC staining of GFAP (magenta), DAPI (cyan), and pan–flavivirus E protein (yellow) in the mice described in (J). n = 8 to 10 mice per group. (**L**) IHC staining of GFAP (magenta), DAPI (cyan), and pan–flavivirus E protein (yellow) in the mice described in (J). Scale bar,  $20 \mu$ m. Images are at  $40 \times$  magnification.  $20 \times 10^{-10}$  Magnification.  $20 \times 10^{-10}$  Days (Pi var) and  $20 \times 10^{-10}$ 

to D). Ripk3<sup>fl/fl</sup> Aldh1l1 Cre<sup>+</sup> mice also exhibited earlier and more pronounced weight loss in the first 6 days of infection in all three models (Fig. 1, B to D), suggesting that astrocytic RIPK3 restricts pathogenesis in these models. We did not observe evidence of haploinsufficiency in *Ripk3*<sup>fl/+</sup> *Aldh1l1* Cre<sup>+</sup> animals, nor did we observe any effect of tamoxifen administration on pathogenesis in mice coexpressing Aldh111 Cre with wild-type Ripk3 alleles (Fig. 1E). As a complementary approach, we also used mice harboring astrocytespecific overexpression of RIPK3 (fig. S1C). This line expresses a chimeric version of RIPK3 (RIPK3-2xFV) under the control of a lox-STOP-lox element in the Rosa26 locus. RIPK3-2xFV features two FKBP<sup>F36V</sup> domains that facilitate enforced oligomerization after treatment with a dimerization drug. This construct leaves the endogenous Ripk3 locus intact, and thus this mouse line can be used as either a cell type-specific overexpression system or an enforced chemogenetic activation system in cell types of interest in vivo (29, 30, 35). Note that mice with astrocyte-specific overexpression of RIPK3 (Ripk3-2xFV<sup>fl/fl</sup> Aldh1l1 Cre<sup>+</sup>) exhibited significant amelioration of disease after intracranial challenge with ZIKV-MR766 (Fig. 1, F and G), further supporting a protective function for astrocytic RIPK3 during flavivirus infection.

We next questioned whether astrocytic RIPK3 promotes host survival through direct suppression of flavivirus replication and brain viral burden. Analysis of ZIKV RNA abundance in brain homogenates showed no differences between Ripk3<sup>fl/fl</sup> Aldh1l1 Cre<sup>+</sup> mice and littermate controls after ZIKV-MR766 infection (Fig. 1H). Multistep growth curve analysis also showed no difference in ZIKV-MR766 replication in primary astrocytes derived from Ripk3<sup>-/-</sup> mice compared to cultures derived from heterozygous littermate controls (Fig. 11). We also saw no differences in replication of either ZIKV-MR766 or WNV-WN02-Bird114 in primary astrocytes treated with GSK872, an inhibitor of RIPK3 kinase function that does not alter its abundance (fig. S1, D to G). Immunohistochemical (IHC) analysis of infected cells in the cerebral cortices of animals infected with ZIKV-MR766 also showed no effect of astrocytic RIPK3 deletion on the numbers of infected neurons (Fig. 1, J and K), which represent most of the infected cells during flavivirus encephalitis (18, 36, 37). Although infection of astrocytes is more sporadic in this model and therefore difficult to systematically quantify, we also did not observe qualitative differences in the location or numbers of infected astrocytes between genotypes (Fig. 1L). We also observed no effect of Mlkl (mixed lineage kinase domain-like pseudokinase) deficiency on ZIKV-MR766 replication (fig. S1H) or of either *Ripk3* or *Mlkl* deficiency on astrocyte viability after infection (fig. S1I), suggesting that RIPK3 does not control ZIKV infection by inducing necroptosis, consistent with our previous work (29). We further confirmed this finding by showing that Mlkl deficiency did not affect pathogenesis in vivo after infection with any of the flavivirus strains used in our study (fig. S1J). We also observed a complete absence of phosphorylated (activated) MLKL in brain homogenates derived from mice infected with ZIKV-MR766 (fig. S1, K and L). Together, these data suggest that the protective benefit of astrocytic RIPK3 was not achieved through induction of MLKLdependent necroptosis, nor was it driven by direct modulation of infection or viral replication in the CNS.

# Activation of astrocytic RIPK3 drives proinflammatory gene expression

Given our observation of a protective function for endogenous RIPK3 activity during flavivirus encephalitis, we next questioned whether

exogenous activation of RIPK3 would have therapeutic efficacy. We thus infected mice expressing the chemogenetically activatable RIPK3-2xFV protein in astrocytes (Ripk3-2xFV<sup>fl/fl</sup> Aldh1l1 Cre<sup>+</sup>) with ZIKV-MR766. Mice were treated on day 3 after infection with B/B homodimerizer (B/B), which drives the dimerization and activation of RIPK3-2xFV, or a vehicle control solution (Fig. 2A). Chemogenetic activation of RIPK3 conferred significant protection from intracranial ZIKV-MR766 challenge, as indicated by essentially complete amelioration of mortality and weight loss in the B/B-treated group (Fig. 2B). Note that this effect occurred in the absence of any detectable activation of MLKL (fig. S2A). To better understand the mechanisms of protection induced by astrocytic RIPK3, we performed magnetic-activated cell sorting (MACS) of ACSA2<sup>+</sup> astrocytes (fig. S2, B and C) 24 hours after B/B administration to Ripk3-2xFV<sup>fl/fl</sup> Aldh111 Cre<sup>+</sup> mice or their Cre<sup>-</sup> littermate controls (Fig. 2C). Sorted astrocytes were subjected to bulk RNA sequencing (RNA-seq). Astrocytes derived from Ripk3-2xFV<sup>fl/fl</sup> Aldh111 Cre<sup>+</sup> mice exhibited robust transcriptomic changes compared with those in astrocytes derived from controls, as evidenced by distinct clustering in principal components analysis (PCA) (Fig. 2D). Chemogenetic RIPK3 activation in astrocytes resulted in 3662 significantly differentially expressed genes (DEGs) in total, including 1691 DEGs that were reduced in expression and 1971 DEGs that were increased in expression (Fig. 2E). Gene Ontology (GO) enrichment analysis revealed significant overrepresentation of terms related to immune cell trafficking and inflammatory signaling, consistent with previous work from our group and others establishing RIPK3 as a key coordinator of neuroinflammation (fig. S2D). Further analysis of selected enriched GO terms revealed predominantly increased expression of genes associated with type I interferon (IFN) signaling (Fig. 2F), cytokine responses (Fig. 2G), and T cell-mediated immunity (Fig. 2H), consistent with an overall proinflammatory transcriptomic signature in the setting of RIPK3 activation. We also confirmed that endogenous *Ripk3* was required for the increased amounts of both transcript and protein of inflammatory chemokines and IFN-stimulated genes in primary astrocyte cultures infected with ZIKV-MR766 (Fig. 2, I and J). Together, these findings demonstrate that both chemogenetic and infection-induced activation of RIPK3 drive proinflammatory gene expression in astrocytes.

# Astrocytic RIPK3 suppresses CNS leukocyte infiltration during flavivirus encephalitis

We previously demonstrated a role for RIPK3 signaling in neurons to drive recruitment of antiviral leukocytes into the CNS through the induction of inflammatory chemokine expression (30). Given that activation of RIPK3 in astrocytes also appeared to drive chemokine expression, we questioned whether astrocytic RIPK3 similarly supported leukocyte recruitment to the CNS. We thus performed flow cytometric analysis of CNS leukocytes on day 4 after intracranial ZIKV-MR766 infection (Fig. 3A and fig. S3A). Unexpectedly, we observed increased percentages of CD45<sup>hi</sup> infiltrating cells in Ripk3<sup>fl/fl</sup> Aldh111 Cre<sup>+</sup> mice compared with littermate controls after infection (Fig. 3B). In contrast, the percentages of CD45<sup>int</sup>CD11b<sup>+</sup> resident microglia were unchanged between genotypes (Fig. 3C). Further profiling revealed enhanced infiltration of several myeloid cell populations in Ripk3<sup>fl/fl</sup> Aldh1l1 Cre<sup>+</sup> mice, including CD11b<sup>+</sup>Ly6c<sup>+</sup> monocytes and CD11b<sup>+</sup>F4/80<sup>+</sup> macrophages, as well as CD11c<sup>+</sup>MHCII<sup>+</sup> dendritic cells (Fig. 3D). In the lymphocyte compartment, we also observed significant increases in the percentages of both CD8<sup>+</sup> and

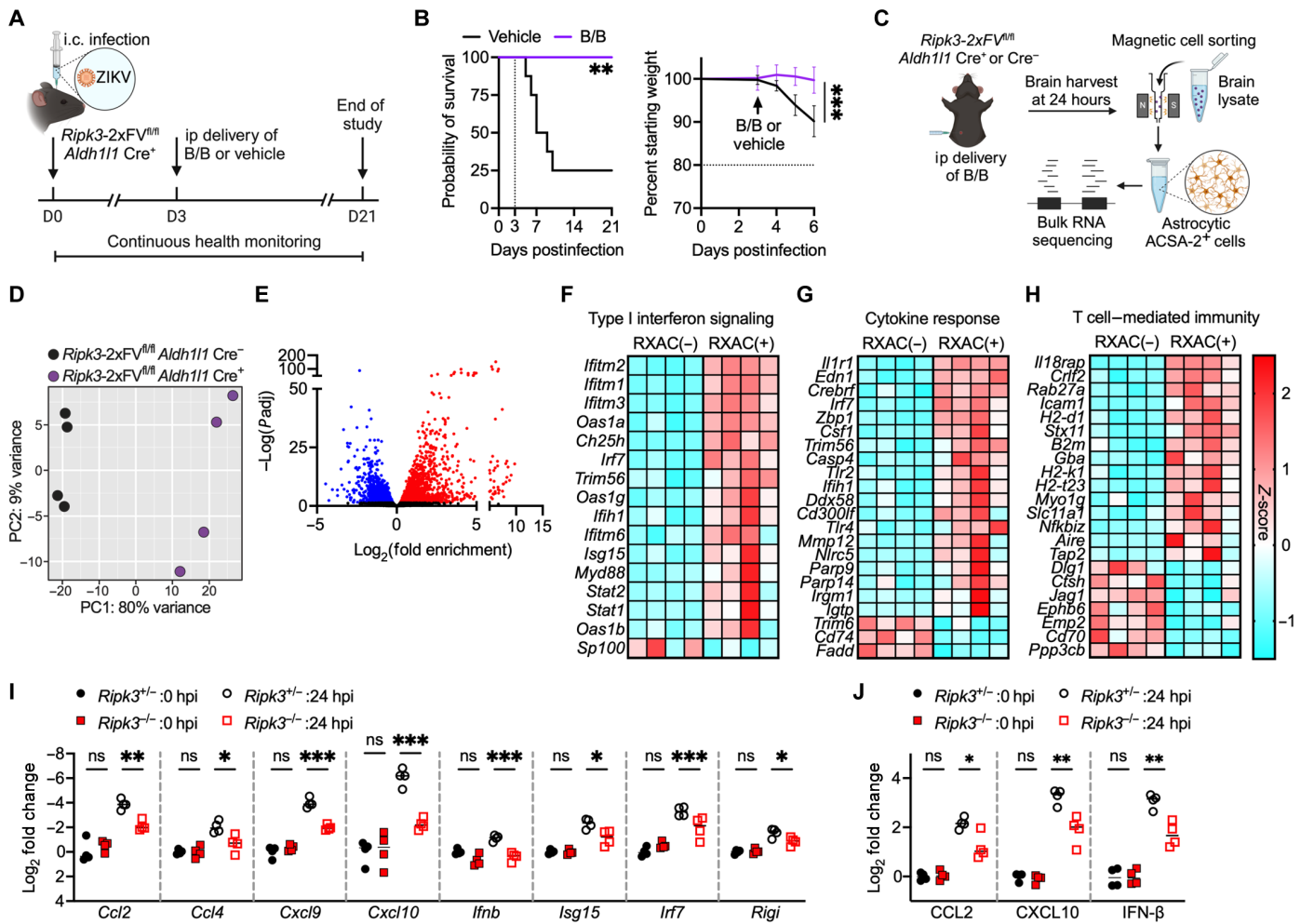


**Fig. 2. Activation of astrocytic RIPK3 induces proinflammatory gene expression.** (**A**) Schematic illustrating survival studies in which mice expressing a chemogenetically activatable form of RIPK3 (Ripk3-2xFV) received intraperitoneal (ip) administration of homodimerizer ligand (B/B) 3 days after high-dose ( $10^3$  PFU) i.c. ZIKV-MR766 infection. D0, day 0. (**B**) Survival and weight measurements in Ripk3-2xFVfl/fl Aldh111 Cre<sup>+</sup> mice treated as described in (A). n = 7 or 8 mice per group. (**C**) Schematic illustrating MACS of ACSA- $2^+$  astrocytes derived from mice of the indicated genotypes 24 hours after intraperitoneal administration of B/B. (**D** and **E**) PCA (D) and volcano plot depicting significant DEGs (E) in bulk RNA-seq data derived from ACSA- $2^+$  astrocytes as described in (C). Transcripts with significant differential expression [>1.5-fold change, adjusted (adj.) P < 0.05] are highlighted. Transcripts reduced in abundance are shown in blue, whereas transcripts increased in abundance are shown in red. n = 4 mice per group. (**F** to **H**) Heatmap depicting significant DEGs within the indicated GO terms. (**I** and **J**) qRT-PCR (I) and ELISA (J) analyses of indicated inflammatory chemokines and IFN-stimulated genes in primary astrocytes derived from mice of the indicated genotypes 0 or 24 hours after ZIKV-MR766 infection. n = 4 cultures per group. \*P < 0.05, \*\*P < 0.05, and \*\*\*P < 0.00, and \*\*P <

CD4<sup>+</sup>T cell subsets, as well as NK1.1<sup>+</sup> natural killer (NK) cells (Fig. 3, E and F). Furthermore, these changes were not due to baseline differences in CNS leukocyte populations between genotypes, because we did not observe differences in any CNS leukocyte subset in mockinfected animals (Fig. 3, C, D, and F, and fig. S3B). We also did not observe differences in non-CNS immune responses, including leukocyte frequencies in the spleen (fig. S3, C and D). These data suggest that, despite promoting the expression of a broad set of traditionally proinflammatory genes, RIPK3 activity in astrocytes nevertheless exerts an anti-inflammatory effect on CNS leukocyte infiltration during flavivirus encephalitis.

# Astrocytic RIPK3 promotes a complex immunologic transcriptional program, including genes encoding multiple serpins

Given these paradoxical findings, we returned to our transcriptomic analysis to assess how astrocytic RIPK3 influences gene pathways associated with anti-inflammatory signaling and immunoregulation. We observed enrichment of several relevant GO terms in our dataset, including "inhibition of inflammatory response" and "inhibition of lymphocyte activation" (Fig. 4A). Analysis of expression patterns within these enriched GO terms revealed complex patterns of both increased and decreased expression, suggesting that RIPK3

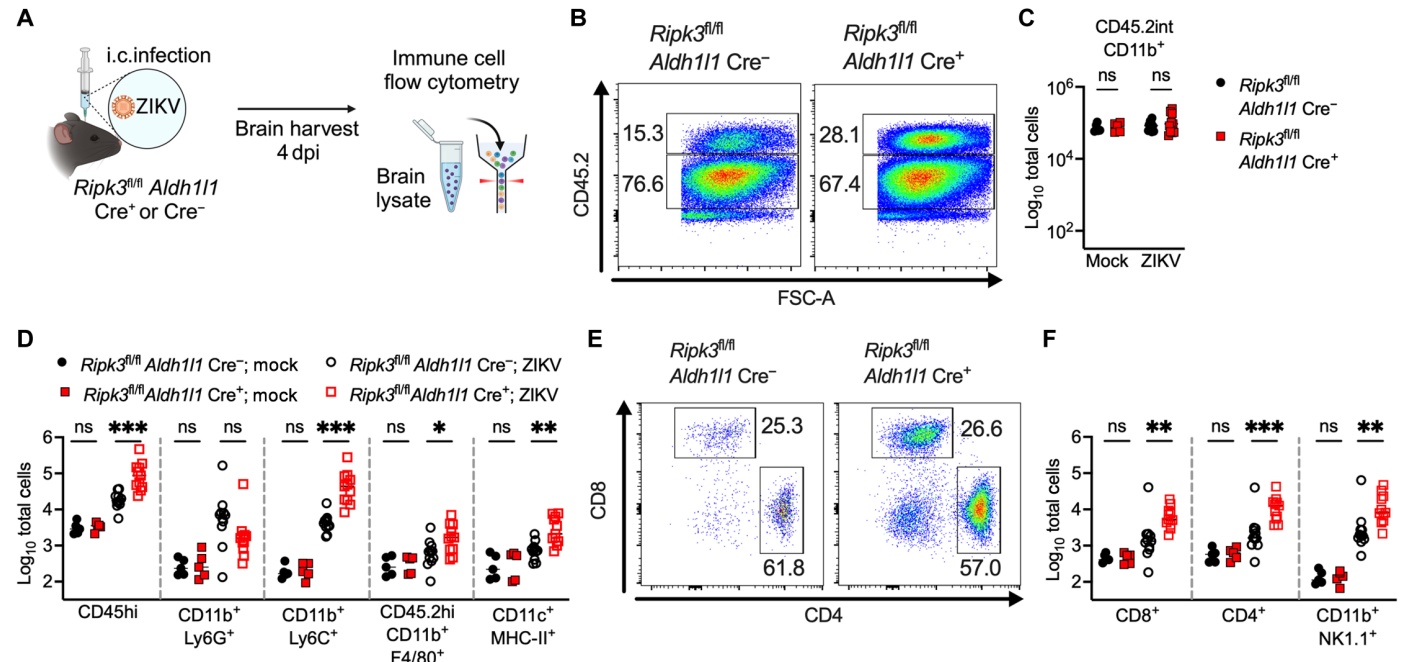


Fig. 3. Astrocytic RIPK3 suppresses CNS leukocyte infiltration during flavivirus encephalitis. (A) Schematic illustrating the flow cytometric analysis of CNS leukocytes derived from mice of the indicated genotypes 4 days after i.c. ZIKV-MR766 infection. dpi, days postinfection. (B) Representative flow cytometry plots depicting resident (CD45.2<sup>int</sup>) or infiltrating (CD45.2<sup>int</sup>) CNS leukocytes derived from mice infected with ZIKV-MR766 as described in (A). (C) Total numbers of CD45<sup>int</sup>CD11b<sup>+</sup> resident microglia in brain tissues derived from mice of the indicated genotypes after ZIKV-MR766 infection. (D) Total numbers of the indicated myeloid cell populations in brain tissues derived from mice of the indicated genotypes after ZIKV-MR766 infection. (E) Representative flow cytometry plots depicting CD4<sup>+</sup> T cells and CD8<sup>+</sup> T cells derived as described for (A). (F) Total numbers of CD8<sup>+</sup> T cells, CD4<sup>+</sup> T cells, and NK1.1<sup>+</sup> NK cells in brain tissues derived from mice of the indicated genotypes after ZIKV-MR766 infection. n = 5 to 11 mice per group in all panels. n = 5 to 11 mice per group in all panels. n = 5 to 11 mice per group in all panels. n = 5 to 11 mice per group in all panels. n = 5 to 11 mice per group in all panels. n = 5 to 12 mice per group in all panels. n = 5 to 13 mice per group in all panels. n = 5 to 15 mice per group in all panels. n = 5 to 16 mice per group in all panels. n = 5 to 17 mice per group in all panels. n = 5 to 18 mice per group in all panels. n = 5 to 19 mice per group in all panels. n = 5 to 19 mice per group in all panels. n = 5 to 19 mice per group in all panels. n = 5 to 19 mice per group in all panels. n = 5 to 19 mice per group in all panels. n = 5 to 19 mice per group in all panels. n = 5 to 19 mice per group in all panels. n = 5 to 19 mice per group in all panels. n = 5 to 19 mice per group in all panels. n = 5 to 19 mice per group in all panels. n = 5 to 19 mice per group in all panels. n = 5 to 19 mice per group in all pan

likely exerts more nuanced control over inflammatory signaling in astrocytes than has been appreciated previously (Fig. 4B and fig. S4). Among the DEGs induced by RIPK3 activation in astrocytes, we noticed that those encoding serpins were particularly enriched, representing 5 of the top 25 DEGs that were increased in expression (Fig. 4C). Serpins constitute a family of endogenous serine protease inhibitors that exert diverse immunoregulatory functions, including inhibition of leukocyte proteases and matrix metalloproteinases (MMPs) that support inflammation (38, 39). These molecules thus stood out to us as a promising candidate mechanism of immunoregulation downstream of astrocytic RIPK3. In total, chemogenetic activation of RIPK3 significantly altered the expression of genes encoding 15 serpins (Fig. 4D). We also confirmed that endogenous Ripk3 was required to induce the expression of serpin-encoding genes in primary mouse astrocyte cultures infected with ZIKV-MR766 (Fig. 4E). We previously showed that RIPK3 activation in astrocytes regulates transcription by activating the inflammatory transcription factor nuclear factor κB (NF-κB) (34, 40). Because many serpins contain  $\kappa B$  elements in their promoters (41–43), we tested a requirement for NF-κB in astrocytic serpin expression with inhibitors of NF-kB signaling, including BAY 11-7085 (an inhibitor of IκB kinase activity) and JSH-23 (an inhibitor of NF-κB p65 nuclear translocation). Both inhibitors abrogated the expression of serpinencoding genes after ZIKV-MR766 infection (Fig. 4E). Together, these data identify serpins as candidate immunoregulatory molecules induced downstream of RIPK3 and NF-κB in astrocytes.

#### SerpinA3N is protective in models of flavivirus encephalitis

Among the differentially expressed serpin-encoding genes in our transcriptomic analysis, we noted *Serpina3n* because of numerous reports of its high expression in astrocytes and involvement in various neurologic diseases (41). We confirmed that SerpinA3N protein abundance was increased in whole-brain homogenates from control animals infected with ZIKV-MR766, whereas this increase was reduced in *Ripk3*<sup>fl/fl</sup> *Aldh111* Cre<sup>+</sup> mice (Fig. 5A). We similarly observed an increase in SerpinA3N protein abundance in the medium of *Ripk3*-sufficient astrocyte cultures after ZIKV-MR766 infection that was significantly reduced in *Ripk3*<sup>-/-</sup> cultures (fig. S5A). We next questioned whether reconstitution of SerpinA3N protein in the CNS of *Ripk3*<sup>fl/fl</sup> *Aldh111* Cre<sup>+</sup> mice would affect disease pathogenesis. We thus performed intracerebroventricular administration of recombinant murine SerpinA3N in mice 2 days after intracranial ZIKV-MR766 infection (Fig. 5B).

Because SerpinA3N is a potent inhibitor of serine protease activity, we first measured overall levels of proteolysis in the brain with an assay that measures endogenous collagenase and gelatinase activity through the cleavage of a fluorogenic gelatin substrate. Brain homogenates from *Ripk3*<sup>fl/fl</sup> *Aldh1l1* Cre<sup>+</sup> mice exhibited significantly enhanced collagenase/gelatinase activity compared with that of littermate controls; however, this effect was reversed after intracerebroventricular injection of SerpinA3N (Fig. 5C). Among the serine proteases inhibited by SerpinA3N in the brain are MMPs and other enzymes that degrade extracellular matrix and tight junction molecules that support BBB

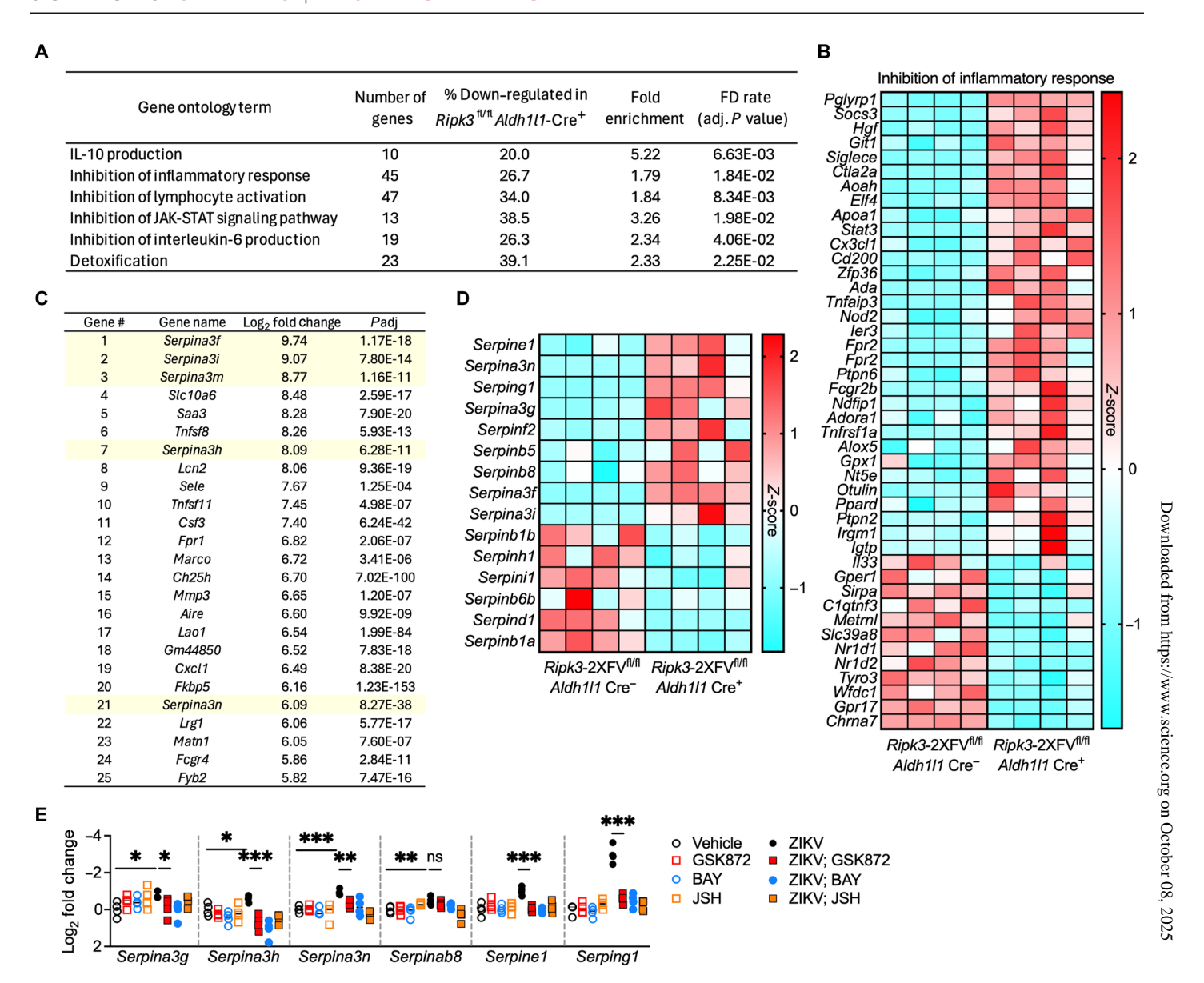


Fig. 4. Astrocytic RIPK3 promotes a complex immunologic transcriptional program, including inducing expression of multiple Serpins. (A) GO enrichment analysis of terms related to anti-inflammatory signaling and immunoregulation, derived from RNA-seq analysis comparing ACSA- $2^+$  astrocytes sorted from Ripk3-2xFVfl/fl Al-dh111 Cre<sup>+</sup> mice with astrocytes sorted from Cre<sup>-</sup> littermate controls 24 hours after B/B treatment. JAK-STAT, Janus kinase–signal transducers and activators of transcription; FD, false discovery. (B) Heatmap depicting significant DEGs within the indicated GO term. (C) The top 25 DEGs induced by chemogenetic RIPK3 activation in ACSA- $2^+$  astrocytes. (D) Heatmap depicting all significantly differentially expressed serpin-encoding genes induced by chemogenetic RIPK3 activation in astrocytes. n = 4 mice per group for (A) to (D). (E) qRT-PCR analysis of the indicated serpin-encoding genes in primary astrocytes derived from C57BL/6J mice. Astrocytes were pretreated for 2 hours with the indicated inhibitors and then were infected with ZIKV-MR766. Gene expression was measured 24 hours after infection. n = 4 cultures per group. \*P < 0.05, \*\*P < 0.01, and \*\*\*P < 0.001. GO enrichment analysis in (A) was performed with a binomial test with Benjamini-Hochberg correction for multiple comparisons. Data in (E) were compared by two-way ANOVA with Tukey's post hoc test.

function. We thus performed immunostaining for the BBB-specific tight junction molecule Claudin-5 and its adaptor ZO-1, which colocalize in brain vascular endothelia under homeostatic conditions. We observed significant perturbation of Claudin-5 and ZO-1 colocalization in *Ripk3*<sup>fl/fl</sup> *Aldh1l1* Cre<sup>+</sup> mice compared with that in controls, which was driven primarily by loss of ZO-1 (Fig. 5, D and E). However, this effect was prevented through the administration of exogenous SerpinA3N. Similarly, we observed that *Ripk3*<sup>fl/fl</sup> *Aldh1l1* Cre<sup>+</sup>

mice exhibited diminished BBB function during infection, as evidenced by increased extravasation of sodium fluorescein into the CNS parenchyma compared with that of controls (Fig. 5F), and this, too, was ameliorated by SerpinA3N.

Given these confirmations that exogenous SerpinA3N could rescue changes in brain protease activity and BBB function in animals lacking astrocytic RIPK3, we next questioned whether this intervention would have clinical efficacy in models of flavivirus encephalitis.

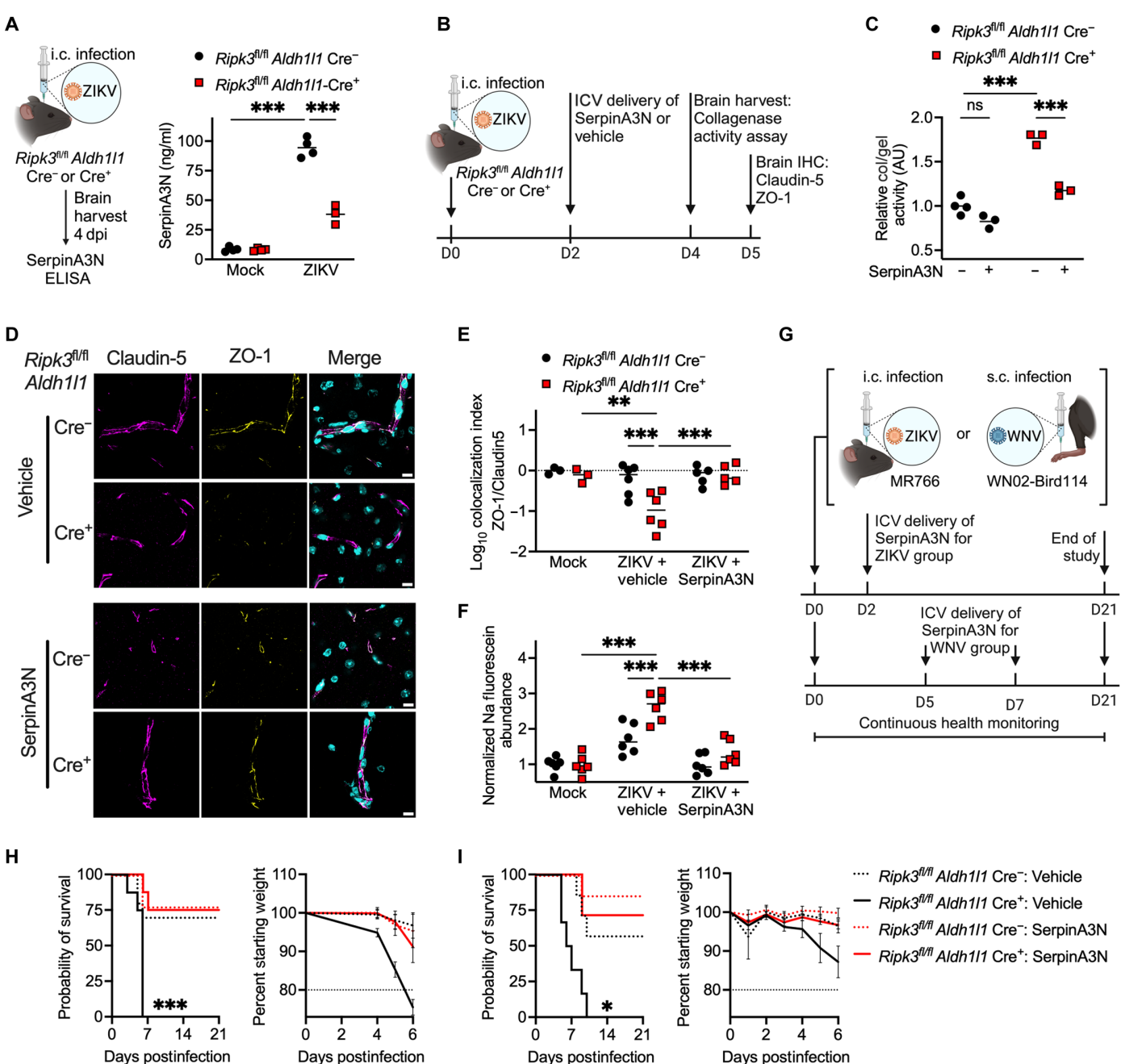


Fig. 5. SerpinA3N is protective in models of flavivirus encephalitis. (A) SerpinA3N concentrations (as measured by ELISA) in whole-brain homogenates derived from mice of the indicated genotypes 4 days after i.c. ZIKV-MR766 infection. n=4 mice per group. (B) Schematic illustrating the timeline of i.c. ZIKV-MR766 infection and intracerebroventricular (ICV) treatment with recombinant SerpinA3N before various end-point readouts. (C) Collagenase/gelatinase (col/gel) activity assay in whole-brain homogenates derived from mice of the indicated genotypes after ZIKV-MR766 infection and SerpinA3N treatment, as described for (B). n=3 or 4 mice per group. AU, arbitrary units. (D) IHC staining of Claudin5 (magenta), ZO-1 (yellow), and DAPI (cyan) in cortical brain tissue of mice of the indicated genotypes after ZIKV-MR766 infection and SerpinA3N treatment, as described for (B). Scale bars, 10  $\mu$ m. Images are at 63× magnification. (E) Colocalization index of Claudin5 and ZO-1 staining in cortical brain sections as described for (D). n=3 to 6 mice per group. (F) BBB permeability was evaluated by quantifying sodium fluorescein accumulation in tissue homogenates obtained from whole brain. Results are expressed as individual brain values normalized to the sodium fluorescein concentration in serum for each mouse. n=6 replicates per group. (G) Schematic illustrating survival studies in which mice received i.c. ZIKV-MR766 infection or s.c. WNV-WN02-Bird114 infection, followed by ICV administration of recombinant SerpinA3N at the indicated intervals after infection. (H and I) Survival and weight measurements in mice of the indicated genotypes after ZIKV-MR766 infection (H) or WNV-WN02-Bird114 infection (I) with or without ICV SerpinA3N treatment, as described for (G). n=6 to 10 mice per group. \*P<0.05, \*\*P<0.01, and \*\*\*P<0.01. Error bars represent SEM. Data in (A) to (F) were compared by two-way ANOVA with Tukey's post hoc test. Survival data in (H) and (I) were compared by log-rank test.

We thus performed intracerebroventricular SerpinA3N administration at times preceding the onset of clinical disease in the setting of intracranial ZIKV-MR766 infection or subcutaneous WNV-WN02-Bird114 infection (Fig. 5G). Injection of SerpinA3N at day 2 after intracranial ZIKV-MR766 infection significantly ameliorated both weight loss and overall animal mortality in *Ripk3*<sup>fl/fl</sup> *Aldh1l1* Cre<sup>+</sup> mice (Fig. 5H). We observed similar results from two injections of SerpinA3N at days 5 and 7 after subcutaneous WNV-WN02-Bird114 infection (Fig. 5I). We note that two injections were used in this model because of the delayed and more protracted course of disease that occurs after subcutaneous (rather than intracranial) infection. Together, these data suggest that SerpinA3N confers protection during flavivirus encephalitis and that reduced SerpinA3N abundance is a mechanism of enhanced disease burden in mice lacking astrocytic RIPK3.

### SerpinA3N suppresses deleterious neuroinflammation during flavivirus encephalitis

We next assessed potential mechanisms by which SerpinA3N ameliorates pathogenesis during flavivirus encephalitis. We found that recombinant SerpinA3N did not have a direct antiviral effect against either ZIKV-MR766 or WNV-WN02-Bird114 in astrocyte cultures in vitro, suggesting that, similar to RIPK3, SerpinA3N does not limit pathogenesis through restriction of viral replication (fig. S5, B and C). In addition to inhibiting MMPs, SerpinA3N inhibits the activities of several proteases involved in inflammatory signaling, including cathepsins, leukocyte elastase, and granzyme B (44), and may also exert immunoregulatory functions through protease-independent mechanisms (41). We thus questioned whether a lack of SerpinA3N might be a driver of enhanced neuroinflammation in Ripk3fl/fl Aldh1l1 Cre+ mice during flavivirus infection. We found that intracerebroventricular delivery of exogenous SerpinA3N 2 days after intracranial ZIKV infection significantly ameliorated the enhanced CNS leukocyte infiltration observed in *Ripk3*<sup>fl/fl</sup> *Aldh1l1* Cre<sup>+</sup> mice (Fig. 6A). This effect occurred across several leukocyte subsets, including both CD4<sup>+</sup> and CD8<sup>+</sup> T cells, NK cells, and monocytes (Fig. 6B). Among these subsets, previous work has established pathogenic roles for infiltrating CD8<sup>+</sup> T cells, in particular, in promoting host mortality during flavivirus encephalitis (18, 19). We therefore questioned whether the enhanced infiltration of CD8<sup>+</sup> T cells was a mechanism underlying the enhanced pathogenesis observed in mice lacking astrocytic RIPK3 after flavivirus infection. To do so, we depleted CD8<sup>+</sup> T cells by administration of an anti-CD8 neutralizing antibody 2 days after intracranial ZIKV-MR766 infection (Fig. 6C). We confirmed complete depletion of circulating CD8+ T cells 2 days later (day 4 after infection) (fig. S6, A and B). CD8<sup>+</sup> T cell depletion significantly ameliorated the enhanced mortality and weight loss observed in Ripk3<sup>fl/fl</sup> Aldh111 Cre<sup>+</sup> mice after infection, confirming a pathogenic role for this cell type in the absence of astrocytic RIPK3 (Fig. 6D). This amelioration of animal mortality in CD8<sup>+</sup> T cell-depleted Ripk3<sup>tl/tl</sup> Aldh111 Cre<sup>+</sup> animals was also associated with decreased signs of neuroinflammation, as indicated by reduced immunoreactivity for glial fibrillary acidic protein (GFAP) in the cerebral cortex (Fig. 6, E and F).

To more directly assess whether SerpinA3N limited CD8<sup>+</sup> T cell-mediated immunopathology, we performed similar experiments in which mice received intracerebroventricular administration of an anti-SerpinA3N neutralizing antibody or isotype control, with or without simultaneous systemic depletion of CD8<sup>+</sup> T cells (Fig. 6G). Neutralization of SerpinA3N in the CNS significantly enhanced animal mortality

after ZIKV-MR766 infection (Fig. 6H). Moreover, this enhanced mortality was rescued by depletion of CD8<sup>+</sup> T cells, suggesting that SerpinA3N confers protection during flavivirus encephalitis by suppressing CD8<sup>+</sup> T cell-mediated mechanisms of pathogenesis. Together, these data support a model in which astrocytic RIPK3 restricts immunopathology during flavivirus encephalitis through the induction of serpin protease inhibitors, such as SerpinA3N, which maintain BBB integrity and suppress deleterious recruitment of pathogenic CD8<sup>+</sup> T cells to the brain.

#### **DISCUSSION**

Previous work broadened our understanding of RIPK3 signaling to include functions beyond its traditional association with necroptosis. The susceptibility of CNS cells to necroptosis is somewhat controversial and appears to depend greatly on the specifics of the disease model being studied (22, 24, 45, 46). Whereas previous work suggests that ZIKV infection can induce necroptosis to restrict viral replication in an immortalized astrocytic cell line (47), our findings here with in vivo mouse genetic tools and primary murine astrocyte cultures suggest that necroptosis is not the outcome of flavivirus infection in astrocytes in these systems. Rather, astrocytic RIPK3 conferred protection against pathogenesis through alternative mechanisms, as we have observed previously in neurons (29–31, 48). To date, the described cell death-independent functions of RIPK3 have primarily been proinflammatory in nature. Within the CNS, we and others have shown that RIPK3 signaling is a central coordinator of neuroinflammatory activation, with both protective and pathologic consequences during neurologic disease states (21, 22, 46). Despite this understanding, cell type-specific functions for RIPK3 within the CNS have not been carefully delineated.

However, emerging evidence does suggest that RIPK3 serves rather distinct functions across CNS cell types during flavivirus infection. We showed previously that neuronal RIPK3 is required for cellintrinsic expression of antiviral effector genes, as well as for the expression of chemokines that recruit infiltrating leukocytes to the CNS during flavivirus infection, and that both of these mechanisms are required for host protection (29–31). Neuronal RIPK3 also appears to confer protection against flavivirus infection through nonimmune mechanisms, such as the suppression of excitotoxic neuronal cell death during flavivirus encephalitis (48). In contrast, we reported that RIPK3 signaling in astrocytes is deleterious in models of parkinsonian neurodegeneration, where it promotes pathogenic neuroinflammation and neurotoxicity (34, 40). Here, we demonstrated a more nuanced role for astrocytic RIPK3 in regulating neuroinflammation during viral encephalitis. Whereas RIPK3 in astrocytes promoted a robust inflammatory transcriptomic signature, it also coordinated expression of immunomodulatory genes that limited the extent of leukocyte infiltration and immunopathology. These data suggest that RIPK3 may also exert more complex regulation of inflammatory processes than was previously appreciated in other cell types, including neurons. Together, our findings underscore the potential for specialized, cell type-specific functions for this pathway in maintaining a balanced and targeted immune response within the CNS.

Our findings also highlight a critical role for astrocytes in the control of protease activity in the CNS, with important implications for BBB integrity and leukocyte recruitment during neuroinflammation. Endogenous proteases, including gelatinases such as MMPs, play important roles in the pathogenesis of flavivirus encephalitis. MMP-9,

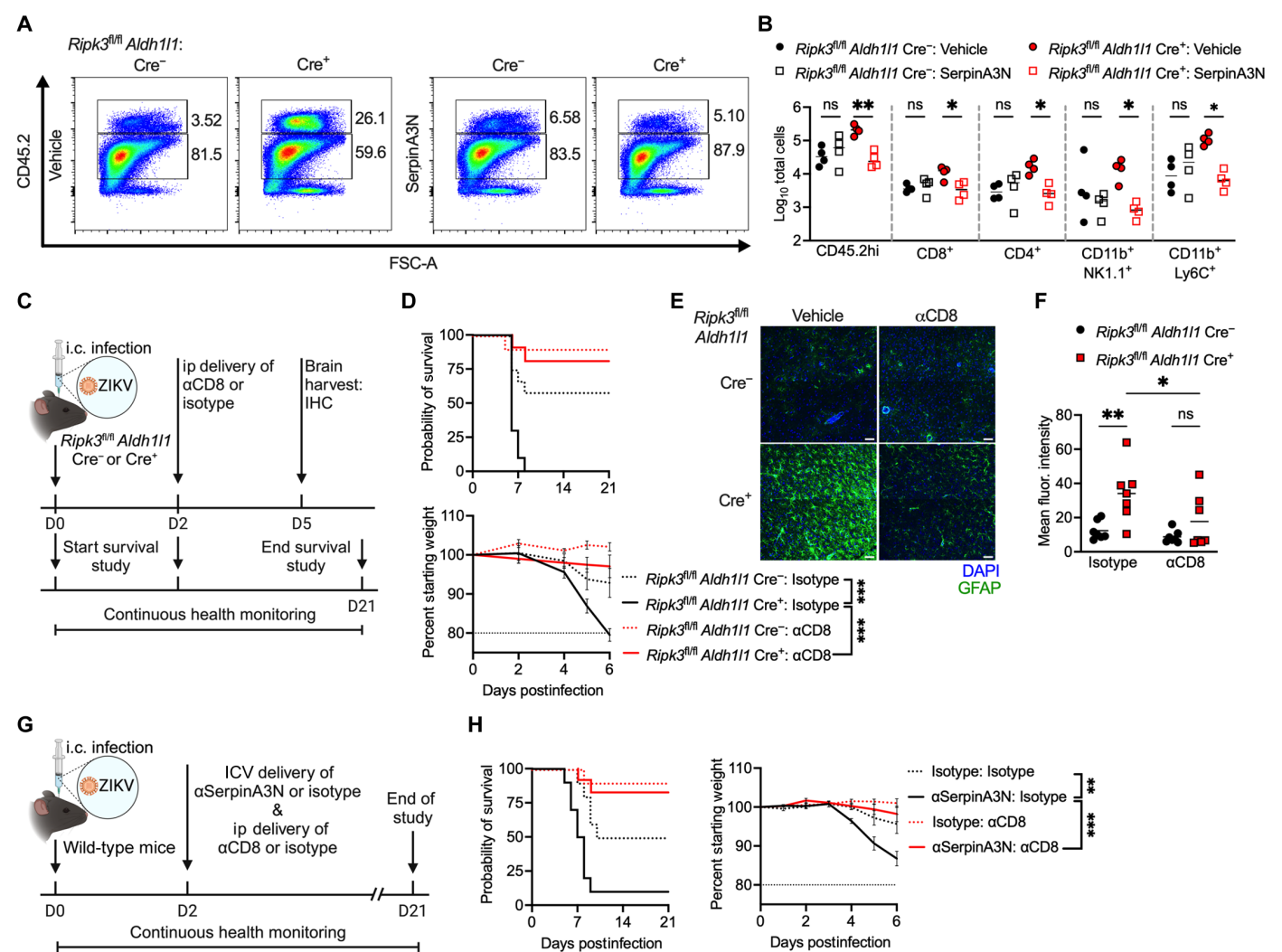


**Fig. 6. SerpinA3N suppresses deleterious neuroinflammation during flavivirus encephalitis.** (**A**) Representative flow cytometry plots depicting resident (CD45.2<sup>int</sup>) and infiltrating (CD45.2<sup>hi</sup>) CNS leukocytes derived from mice of the indicated genotypes infected with ZIKV-MR766 with or without ICV treatment with SerpinA3N 2 days after infection. Flow cytometry analysis was performed 4 days after infection. (**B**) Total numbers of the indicated leukocyte populations in brain tissue derived from the mice described in (A). n = 4 mice per group. (**C**) Schematic illustrating survival study and IHC analysis in which mice received intraperitoneal administration of an anti-CD8 neutralizing antibody (αCD8) 2 days after i.c. ZIKV-MR766 infection. (**D**) Survival and weight measurements in mice of the indicated genotypes after ZIKV-MR766 infection with or without depletion of CD8<sup>+</sup> T cells, as described for (C). n = 7 to 9 mice per group. (**E**) IHC analysis of GFAP (green) and DAPI (blue) in cortical brain tissues derived from mice of the indicated genotypes treated as described for (C). Images are 2 × 2 tiled composites at 20× magnification. Scale bars, 50 μm. (**F**) Mean fluorescence intensity values of GFAP staining in cortical brain tissues derived from mice of the indicated genotypes and treated as described for (C). n = 7 mice per group. (**G**) Schematic illustrating survival study in which mice received intraperitoneal administration of anti-SerpinA3N (αSerpinA3N) and anti-CD8 neutralizing antibodies (αCD8) 2 days after i.c. ZIKV-MR766 infection. (**H**) Survival and weight measurements in mice of the indicated genotypes after ZIKV-MR766 infection with or without depletion of SerpinA3N and CD8<sup>+</sup> T cells, as described for (G). n = 10 mice per group. \*P < 0.05 and \*\*P <

for example, is increased in abundance during flavivirus encephalitis and contributes to BBB breakdown by degrading tight junction proteins and extracellular matrix components, such as collagen (49–51). This proteolytic activity facilitates the infiltration of immune cells into the CNS, exacerbating neuroinflammation and tissue damage (52, 53). Similarly, granzyme B is a serine protease released by cytotoxic T cells and NK cells and is increased in abundance in brain-infiltrating lymphocytes during flavivirus encephalitis (13, 54–56). In addition to its role in degrading BBB components, granzyme B is a substantial source of immunopathology because of its intrinsic neurotoxic activity

(57–60). These activities highlight the need for tight regulation of inflammatory protease activity to balance effective antiviral immune responses with the preservation of CNS homeostasis.

Our study suggests that protease regulation through serpins, and particularly SerpinA3N, is essential for maintaining acceptable levels of gelatinase activity and preserving BBB tight junctions during flavivirus encephalitis. These findings are consistent with previous reports showing that SerpinA3N effectively protects mice from excessive neuroinflammation and promotes functional recovery in models of ischemic stroke, traumatic brain injury, and multiple

sclerosis (61-65). However, the role of SerpinA3N in the CNS appears to be quite complex, with a range of studies reporting both beneficial (61-66) and detrimental (67-70) effects in different disease contexts. This complexity can probably be partially attributed to the diverse interaction partners of SerpinA3N, which include a broad array of serine proteases (44) as well as nonprotease targets (41). Identifying specific proteases whose inhibition is key to the disease-modifying effects of serpin activity has been a challenge thus far and is a key future direction for our work. Several other variables, including extracellular versus intracellular sites of action, may also underlie the differential effects of serpins in distinct disease contexts (41, 71). The pleotropic nature of the serine protease targets of SerpinA3N may also underlie some of these apparently contradictory findings; for example, target proteases, such as ADAM10/17, MMP-9, and the tPA/plasmin system, not only have major roles in promoting inflammatory responses but also fulfill critical homeostatic functions in the CNS (72–76). The effect of SerpinA3N and related protease inhibitors is thus likely influenced by the context of their expression and the relative abundance, localization, and functional status of the proteases that they target across diverse disease states. New tools enabling cell type-specific genetic manipulation of individual serpins and/or specific serpin-protease interactions will be required to fully clarify and distinguish the beneficial and harmful effects of proteases and their inhibitors in CNS health and disease.

Our study also adds to a growing awareness of the pathogenic role of CD8<sup>+</sup> T cells in the brain during viral encephalitis. Past work suggests that some amount of cytotoxic lymphocyte response in the brain is required for viral clearance and host survival during flavivirus encephalitis (77–79). However, interventions that suppress CD8<sup>+</sup> T cell infiltration and activity in the brain have been shown, paradoxically, to improve host survival and ameliorate neuropathogenesis, without sacrificing virologic control (18, 19, 36). T cell responses in the CNS are under complex regulation, and the balance of their protective versus pathogenic activities is also likely highly context dependent. For example, past work showed that the release of CD8<sup>+</sup> T cells from perivascular spaces by antagonizing the chemokine receptor CXCR4 facilitated their access to parenchymal antigen, which improved viral clearance and diminished immunopathology (80). Similarly, the activation state of antigen-presenting cells within the CNS influences the local reactivation of antigen-specific lymphocytes, optimizing their effector function to promote virologic control and minimize off-target effects on sensitive bystander cells (55). We speculate that the activity of SerpinA3N may influence lymphocyte recruitment in ways that preserve CD8<sup>+</sup> T cell-mediated protection while suppressing the recruitment or aberrant activation of neuropathogenic lymphocytes. This would represent an intriguing mechanism of cross-talk between neurons and astrocytes during flavivirus encephalitis, with neuronal RIPK3 signaling largely promoting CD8<sup>+</sup> T cell recruitment, whereas astrocytic RIPK3 limits and/or optimizes this response to promote neuroprotection over neuropathogenesis.

#### **MATERIALS AND METHODS**

#### **Mouse lines**

All mice in this study were bred and housed under specific pathogen-free conditions in Nelson Biological Laboratories at Rutgers University. All lines were backcrossed to be congenic to the C57BL/6J background (the Jackson Laboratory, no. 000664). Adult (>8-week-old) animals of both sexes were used in all studies, following protocols approved by

the Rutgers University Institutional Animal Care and Use Committee (protocol 201900016). *Ripk3*<sup>-/-</sup> and *Ripk3*<sup>fl/fl</sup> mouse lines were provided by Genentech Inc. (San Francisco, CA, USA). *Mlkl*<sup>-/-</sup> (81) and *Ripk3*-2xFV<sup>fl/fl</sup> (30) lines were provided by A. Oberst (University of Washington, Seattle, WA, USA). *Aldh1l1*-Cre/ERT2 mice were obtained from the Jackson Laboratory (no. 031008), and all animals expressing this transgene were treated intraperitoneally for 5 days with tamoxifen (60 mg/kg; Sigma-Aldrich, no. T5648) in sunflower oil (Sigma-Aldrich, no. S5007). Mice were used for experiments 1 to 2 weeks after the final administration of tamoxifen.

#### Viruses and virologic assays

ZIKV-MR766 was provided by the World Reference Center for Emerging Viruses and Arboviruses. ZIKV-Fortaleza was provided by A. Oberst (University of Washington, Seattle, WA, USA). WNV strain WN02-Bird 114 (82) was provided by B. B. Herrera (Rutgers Robert Wood Johnson Medical School, New Brunswick, NJ, USA). Viral stocks were generated by infecting Vero cells (American Type Culture Collection, no. CCL-81) at a multiplicity of infection of 0.01 and harvesting supernatants at 72 hours after infection. Viral titers of stocks were determined by plaque assay on Vero cells. Cells were maintained in Dulbecco's modified Eagle's medium (Corning, no. 10-013-CV) supplemented with 10% heat-inactivated fetal bovine serum (FBS; Gemini Biosciences, no. 100-106), 1% penicillin-streptomycinglutamine (Gemini Biosciences, no. 400-110), 1% amphotericin B (Gemini Biosciences, no. 400-104), 1% nonessential amino acids (Cytiva, no. SH30238.01), and 1% Hepes (Cytiva, no. SH30237.01). Plaque assay medium was composed of 1× EMEM (Lonza, no. 12-684F) supplemented with 2% heat-inactivated FBS (Gemini Biosciences, no. 100-106), 1% penicillin-streptomycin-glutamine (Gemini Biosciences, no. 400-110), 1% amphotericin B (Gemini Biosciences, no. 400-104), 1% nonessential amino acids (Cytiva, no. SH30238.01), 1% Hepes (Cytiva, no. SH30237.01), 0.75% sodium bicarbonate (VWR, no. BDH9280), and 0.5% methyl cellulose (VWR, no. K390). Plaque assays were developed at 4 days after infection by removal of overlay medium and staining/fixation with 10% neutral buffered formalin (VWR, no. 89370) and 0.25% crystal violet (VWR, no. 0528). Plaque assays were performed by adding 100 µl of serially diluted sample for 1 hour at 37°C to 12-well plates containing 200,000 Vero cells per well. Plates were further incubated with plaque assay medium at 37°C and 5% CO2 for 5 days. Medium was removed from the wells and replaced with fixative containing crystal violet for ~20 to 30 min. Plates were washed repeatedly in H<sub>2</sub>O and allowed to dry before visible plaques were counted.

#### Mouse infections and tissue harvesting

Isoflurane anesthesia was used for all procedures. Unless otherwise noted, mice were inoculated subcutaneously (50  $\mu$ l) with 3  $\times$  10<sup>4</sup> plaque-forming units (PFUs) of WNV-WN02-Bird114 or intracranially (10  $\mu$ l) with 50 PFUs of ZIKV-MR766/ZIKV-Fortalea. Infected mice were monitored by a blinded operator daily for weight loss and presentation of clinical signs of disease, including hunched posture, ruffled fur, hindlimb weakness, and paresis. Mice reaching a moribund state or losing more than 20% of their initial body weight were euthanized, and the date of euthanasia was recorded for the purpose of survival studies. In some experiments, mice underwent cardiac perfusions with 30 ml of cold sterile 1× phosphate-buffered saline (PBS). Extracted tissues were weighed and homogenized with 1.0-mm-diameter zirconia/silica beads (Biospec Products, no.

11079110z) in sterile PBS for plaque assays or with TRI Reagent (Zymo, no. R2050-1) for gene expression analysis. Homogenization was performed in an Omni Beadrupter Elite for two sequential cycles of  $20 \, \mathrm{s}$  at a speed of  $4 \, \mathrm{m/s}$ .

#### **Primary cell culture**

Primary cortical astrocytes were generated from postnatal day 1 (P1) to P3 mouse pups, as previously described (34). Tissues were dissociated with the Neural Dissociation Kit (T) according to the manufacturer's instructions (Miltenyi, no. 130-093-231). Astrocytes were expanded in AM-a medium (ScienCell, no. 1831) supplemented with 10% FBS in fibronectin-coated cell culture flasks and seeded into plates coated with poly-L-lysine ( $20~\mu g/ml$ ; Sigma-Aldrich, no. 9155) before experiments.

#### Magnetic-activated cell sorting

MACS was performed with commercial kits according to the manufacturer's instructions. Mouse brains were dissociated with an Adult Brain Dissociation Kit (Miltenyi, 130-107-677), and isolations were performed with microbead kits designed to isolate astrocytes (Miltenyi, 130-097-678), neurons (Miltenyi, 130-115-389), and myeloid cells (Miltenyi, 130-126-725).

#### **Quantitative real-time PCR**

Total RNA from harvested tissues was extracted with a Zymo Direct-zol RNA Miniprep kit, according to the manufacturer's instructions (Zymo, no. R2051). Total RNA extraction from cultured cells, cDNA synthesis, and subsequent quantitative real-time polymerase chain reaction (qRT-PCR) were performed as previously described (34, 83). Cycle threshold (CT) values for analyzed genes were normalized to the CT values of the housekeeping gene 18S (CT<sub>Target</sub> - CT<sub>18S</sub> =  $\Delta$ CT). Data from primary cell culture experiments were further normalized to baseline control values [ $\Delta$ CT<sub>experimental</sub> -  $\Delta$ CT<sub>control</sub> =  $\Delta$ CT (DDCT)]. Primer sequences for qRT-PCR analysis are shown in table S1.

#### **Bulk RNA-seq**

Ripk3-2XFV<sup>fl/fl</sup> Aldh111 Cre<sup>+</sup> mice and Cre<sup>-</sup> littermate controls were treated intraperitoneally with B/B (Takara, no. AP20187) for 24 hours before perfusion with PBS and harvesting of whole brains. Brains were digested, and myelin was removed with the Adult Brain Dissociation Kit (Miltenyi, no. 130-107-677). Astrocytes were isolated with the Anti–ACSA-2 MicroBead Kit (Miltenyi, no. 130-097-678), and RNA was extracted with the RNeasy Micro Kit (QIAGEN, no. 74004). RNA library preparation, sequencing, and preliminary analysis were performed as described previously (48) by Azenta Life Sciences.

#### Flow cytometry

Mouse brains were dissected from freshly perfused mice and placed into tubes containing  $1\times$  PBS. Brain tissues were incubated with 10 ml of buffer containing 0.05% collagenase type I (Sigma-Aldrich, no. C0130), deoxyribonuclease I (10 µg/ml; Sigma-Aldrich, no. D4527), and 10 mM Hepes (Cytiva, no. SH30237.01) in  $1\times$  Hanks' balanced salt solution (VWR, no. 02-1231-0500) for 1 hour at room temperature under constant rotation. Brain tissues were transferred to a 70-µm strainer on 50-ml conical tubes and mashed through the strainer using the plunger of 3- to 5-ml syringes. Tissue was separated in 8 ml of 37% Isotonic Percoll (Percoll: Cytiva, no. 17-0891-02; RPMI 1640: Corning, no. 10-040-CV, supplemented with 5% FBS)

by centrifugation at 1200g for 30 min with a slow brake. The myelin layer and supernatant were discarded. Leukocytes were incubated in 1× red blood cell (RBC) lysis buffer (Tonbo Biosciences, no. TNB-4300-L100) for 10 min at room temperature. Cells were centrifuged and resuspended in fluorescence-activated cell sorting (FACS) buffer composed of 1× PBS, 0.2% sodium azide, and 5% FBS. Samples were transferred into a U-bottomed 96-well plate. Leukocytes were blocked with 2% normal mouse serum and 1% FcX Block (BioLegend, no. 101320) in FACS buffer for 30 min at 4°C before being stained with Zombie NIR (BioLegend, no. 423105) for 15 min at room temperature. Cells were then stained with fluorescently conjugated antibodies against CD3e (BioLegend, clone 17A2, RRID:AB\_627010), CD44 (BioLegend, clone IM7, RRID:AB\_2890141), CD8a (BioLegend, clone 53-6.7), CD4 (BioLegend, clone RM4-5, RRID:AB\_627057), CD45.2 (BioLegend, clone 104, RRID:AB\_629086), MHC-II (BioLegend, clone M5/114.15.2, RRID:AB 2922924), NK1.1 (BioLegend, clone PK136, RRID:AB\_630043), CD11c (BioLegend, clone N418, RRID:AB\_ 927480), F4/80 (BioLegend, clone BM8, RRID:AB\_469792), CD11b (BioLegend, clone M1/70, RRID:AB\_2536062), Ly6G (BioLegend, clone 1A8, RRID:AB\_2876003), Ly6C (BioLegend, clone HK1.4, RRID:AB\_627896), and CD80 (BioLegend, clone 16-10A1, RRID:AB\_ 2876030). Leukocytes were stained for 30 min at 4°C before washing in FACS buffer and fixation with 1% paraformaldehyde (PFA) in PBS (Thermo Fisher Scientific, no. J19943-K2). Data collection and analysis were performed with a Cytek Northern Lights Cytometer (Cytek) and FlowJo software (Treestar). Data were normalized using a standard bead concentration counted by the cytometer with each sample (Thermo Fisher Scientific, no. C36950). Spleens were crushed between two slides, filtered through a 70-µm cell strainer, and washed with FACS buffer. Isolated splenocytes were incubated with 1× RBC lysis buffer as was done for leukocytes isolated from the brain before blocking and staining were performed.

#### In vivo assessment of BBB permeability

BBB permeability was assessed by the sodium fluorescein leakage assay, as previously described (18, 31). Briefly, mice were injected intraperitoneally with 100 µl of fluorescein sodium salt (100 mg/ml; Sigma-Aldrich, F6377) dissolved in sterile PBS. After 45 min, blood was collected, and the mice were perfused with PBS. Serum and supernatants from homogenized brain tissues were incubated overnight at 4°C in 2% trichloroacetic acid solution (Sigma-Aldrich, T0699) at a 1:1 dilution. Precipitated protein was pelleted by centrifugation at 2823g for 10 min at 4°C. Supernatants were diluted with borate buffer (pH 11) (Sigma-Aldrich, 1094621000) to achieve a neutral pH. Fluorescein emission at 538 nm was measured for samples in an optically clear black-walled 96-well plate (Corning, 3904) with a SpectraMax iD3 plate reader (Molecular Devices). Tissue fluorescence values were standardized against plasma values for individual mice.

#### CD8<sup>+</sup> T cell depletion

To deplete CD8<sup>+</sup> T cells, mice were injected intraperitoneally with 450  $\mu$ g of anti-CD8 antibody (Thermo Fisher Scientific, clone H35-17.2, RRID:AB\_2075781). Blood samples were collected retro-orbitally 2 days later, and circulating leukocytes were assessed by flow cytometry to confirm the depletion of CD8<sup>+</sup> cells.

#### SerpinA3N and anti-SerpinA3N treatment

Mice were injected intracerebroventricularly (-0.3 anterior-posterior; +1.0 medio-lateral; +2.5 dorso-ventral) with 4 ng of recombinant mouse

SerpinA3N protein (R&D Systems, 4709-PI-010) diluted in Hanks' balanced salt solution. Alternatively, mice were injected intracere-broventricularly with 40 ng of anti-SerpinA3N antibody (R&D Systems, AF4709, RRID:AB\_2270116). Doses of recombinant protein and neutralizing antibody were chosen to roughly approximate the concentrations of endogenous SerpinA3N protein detected in control brains during viral encephalitis (Fig. 5A) and to provide an ~10:1 molar ratio of antibody to target protein for efficient neutralization. Primary astrocyte cultures were treated with recombinant mouse SerpinA3N (40 ng/ml) 1 hour before infection for virologic assays.

#### Gelatinase-collagenase activity assay

The EnzCheck Gelatinase/Collagenase Assay Kit (Thermo Fisher Scientific, E12055) was used according to the manufacturer's protocol. Mice were perfused at 4 days after infection with cold sterile 1× PBS, followed by harvesting of the brain. A sagittal cut divided the brain into two halves, one of which was homogenized in 1× reaction buffer. Brain homogenate was centrifuged at 15,000g for 10 min at 4°C, and clarified supernatants were used for the assay. Samples were incubated with fluorogenic gelatin substrate in a black-walled 96-well plate for 2 hours at room temperature. Samples were read on a microplate reader at 485/535 nm.

#### **Enzyme-linked immunosorbent assay**

The following proteins were detected with commercial enzymelinked immunosorbent assay (ELISA) kits according to manufacturers' instructions: SerpinA3N ELISA kit (RayBiotech, ELM-SERPINA3N-1), phosph-MLKL (Ser<sup>345</sup>) ELISA kit (RayBiotech, PEL-MLKL-S345-1), CXCL10 (Thermo Fisher Scientific, BMS6018), CCL2 (Affymetrix, 88-7391-76), and IFN- $\beta$  (Thermo Fisher Scientific, 424001).

#### Immunofluorescence imaging

To image tight junctions, mice were perfused with 30 ml of 1× PBS followed by cold methanol. Brains were placed in methanol overnight and rehydrated in 1× PBS. For other stains, mice were perfused with 30 ml of cold 1× PBS, followed by freshly prepared 4% PFA in 1× PBS. Brains were stored at 4°C overnight, followed by replacement of PFA with 1× PBS until sectioning was performed. In all cases, brains were embedded in agar and sectioned with a compresstome (Presisionary, VF-510-0Z). Sections were blocked with 10% goat or donkey serum with 0.4% Triton X-100, followed by incubation with primary antibodies for 48 hours at 4°C. Antibodies used were as follows: NeuN (1:500; Synaptic Systems, 266-004, RRID:AB\_2619988), pan-flavivirus E protein antibody (1:100; VWR Enzo, 76285-044), GFAP (1:250; Invitrogen, 13-0300, RRID:AB\_86543), Claudin-5 (1:200; Invitrogen, 34-1600, RRID:AB 2533157), and ZO-1 (1:200; Millipore, MABT11, RRID:AB\_10616098). Sections were washed before incubation for 1 hour at room temperature with secondary antibodies. Sections were stained with 4',6-diamidino-2-phenylindole (DAPI) before mounting with ProLong Diamond Antifade (Thermo Fisher Scientific, P36970).

#### Statistical analysis

Statistical analyses were performed with GraphPad Prism 9. Survival experiments were compared by log-rank test. Most other experiments were compared with appropriate parametric tests, including the Student's t test (two-tailed) or two-way analysis of variance (ANOVA) with Tukey's post hoc test to identify significant differences between groups. P < 0.05 was deemed to indicate statistical significance. Unless specified otherwise, all data points represent

biological replicates consisting of distinct mice or independent cultures derived from distinct mice. Unless specified otherwise, all experiments represent values collected from at least two independent experiments. No data points were excluded or omitted from any analysis.

#### **Supplementary Materials**

The PDF file includes:

Figs. S1 to S6 Table S1

Other Supplementary Material for this manuscript includes the following: MDAR Reproducibility Checklist

#### REFERENCES AND NOTES

- M. A. Espinal, J. K. Andrus, B. Jauregui, S. H. Waterman, D. M. Morens, J. I. Santos, O. Horstick, L. A. Francis, D. Olson, Emerging and reemerging *Aedes*-transmitted arbovirus infections in the region of the Americas: Implications for health policy. *Am. J. Public Health* 109, 387–392 (2019).
- H. M. Lazear, E. M. Stringer, A. M. de Silva, The emerging Zika virus epidemic in the Americas: Research priorities. JAMA 315, 1945–1946 (2016).
- H. Asad, D. O. Carpenter, Effects of climate change on the spread of zika virus: A public health threat. Rev. Environ. Health 33, 31–42 (2018).
- D. Musso, A. I. Ko, D. Baud, Zika virus infection—After the pandemic. N. Engl. J. Med. 381, 1444–1457 (2019).
- R. D. Pardy, M. J. Richer, Zika virus pathogenesis: From early case reports to epidemics. Viruses 11, 886 (2019).
- S. E. Ronca, J. C. Ruff, K. O. Murray, A 20-year historical review of West Nile virus since its initial emergence in North America: Has West Nile virus become a neglected tropical disease? PLOS Negl. Trop. Dis. 15, e0009190 (2021).
- L. D. Kramer, A. T. Ciota, A. M. Kilpatrick, Introduction, spread, and establishment of West Nile virus in the Americas. J. Med. Entomol. 56, 1448–1455 (2019).
- H. Patel, B. Sander, M. P. Nelder, Long-term sequelae of West Nile virus-related illness: A systematic review. *Lancet Infect. Dis.* 15, 951–959 (2015).
- A. Y. Vittor, M. Long, P. Chakrabarty, L. Aycock, V. Kollu, S. T. DeKosky, West Nile virus-induced neurologic sequelae-relationship to neurodegenerative cascades and dementias. *Curr. Trop. Med. Rep.* 7, 25–36 (2020).
- B. M. Blackhurst, K. E. Funk, Molecular and cellular mechanisms underlying neurologic manifestations of mosquito-borne flavivirus infections. Viruses 15, 2200 (2023).
- A. M. Bifani, K. W. K. Chan, D. Borrenberghs, M. J. A. Tan, W. W. Phoo, S. Watanabe,
  O. Goethals, S. G. Vasudevan, M. M. Choy, Therapeutics for flaviviral infections. *Antiviral Res.* 210, 105517 (2023).
- T. C. Pierson, M. S. Diamond, The continued threat of emerging flaviviruses. *Nat. Microbiol.* 5, 796–812 (2020).
- N. Chotiwan, E. Rosendal, S. M. A. Willekens, E. Schexnaydre, E. Nilsson, R. Lindqvist, M. Hahn, I. S. Mihai, F. Morini, J. Zhang, G. D. Ebel, L.-A. Carlson, J. Henriksson, U. Ahlgren, D. Marcellino, A. K. Överby, Type I interferon shapes brain distribution and tropism of tick-borne flavivirus. *Nat. Commun.* 14, 2007 (2023).
- A. G. Spiteri, C. L. Wishart, D. Ni, B. Viengkhou, L. Macia, M. J. Hofer, N. J. C. King, Temporal tracking of microglial and monocyte single-cell transcriptomics in lethal flavivirus infection. *Acta Neuropathol. Commun.* 11, 60 (2023).
- L. Yang, J. Xiong, Y. Liu, Y. Liu, X. Wang, Y. Si, B. Zhu, H. Chen, S. Cao, J. Ye, Single-cell RNA sequencing reveals the immune features and viral tropism in the central nervous system of mice infected with Japanese encephalitis virus. J. Neuroinflammation 21. 76 (2024).
- S. Ai, R. S. Klein, Update on T cells in the virally infected brain: Friends and foes. Curr. Opin. Neurol. 33, 405–412 (2020).
- O. Constant, G. Maarifi, F. P. Blanchet, P. Van de Perre, Y. Simonin, S. Salinas, Role of dendritic cells in viral brain infections. Front. Immunol. 13, 862053 (2022).
- B. P. Daniels, H. Jujjavarapu, D. M. Durrant, J. L. Williams, R. R. Green, J. P. White, H. M. Lazear, M. Gale Jr., M. S. Diamond, R. S. Klein, Regional astrocyte IFN signaling restricts pathogenesis during neurotropic viral infection. *J. Clin. Invest.* 127, 843–856 (2017).
- K. J. Szretter, B. P. Daniels, H. Cho, M. D. Gainey, W. M. Yokoyama, M. Gale Jr., H. W. Virgin, R. S. Klein, G. C. Sen, M. S. Diamond, 2'-O methylation of the viral mRNA cap by West Nile virus evades ifit1-dependent and -independent mechanisms of host restriction in vivo. *PLOS Pathog.* 8, e1002698 (2012).
- S. W. van Leur, T. Heunis, D. Munnur, S. Sanyal, Pathogenesis and virulence of flavivirus infections. Virulence 12, 2814–2838 (2021).
- 21. J. P. Angel, B. P. Daniels, Paradoxical roles for programmed cell death signaling during viral infection of the central nervous system. *Curr. Opin. Neurobiol.* **77**, 102629 (2022).

#### SCIENCE SIGNALING | RESEARCH ARTICLE

- B. P. Daniels, A. Oberst, Outcomes of RIP kinase signaling during neuroinvasive viral infection. Curr. Top. Microbiol. Immunol. 442, 155–174 (2023).
- L. Wu, J. Y. Chung, T. Cao, G. Jin, W. J. Edmiston III, S. Hickman, E. S. Levy, J. A. Whalen, E. S. L. Abrams, A. Degterev, E. H. Lo, L. Tozzi, D. L. Kaplan, J. El Khoury, M. J. Whalen, Genetic inhibition of RIPK3 ameliorates functional outcome in controlled cortical impact independent of necroptosis. *Cell Death Dis.* 12, 1064 (2021).
- H. Guo, H. S. Koehler, E. S. Mocarski, R. D. Dix, RIPK3 and caspase 8 collaborate to limit herpes simplex encephalitis. PLOS Pathog. 18, e1010857 (2022).
- R. Peng, C. K. Wang, X. Wang-Kan, M. Idorn, M. Kjaer, F. Y. Zhou, B. K. Fiil, F. Timmermann, S. L. Orozco, J. McCarthy, C. S. Leung, X. Lu, K. Bagola, J. Rehwinkel, A. Oberst, J. Maelfait, S. R. Paludan, M. Gyrd-Hansen, Human ZBP1 induces cell death-independent inflammatory signaling via RIPK3 and RIPK1. EMBO Rep. 23, e55839 (2022).
- M. Najjar, D. Saleh, M. Zelic, S. Nogusa, S. Shah, A. Tai, J. N. Finger, A. Polykratis, P. J. Gough, J. Bertin, M. Whalen, M. Pasparakis, S. Balachandran, M. Kelliher, A. Poltorak, A. Degterev, RIPK1 and RIPK3 kinases promote cell-death-independent inflammation by Toll-like receptor 4. *Immunity* 45, 46–59 (2016).
- M. Zelic, F. Pontarelli, L. Woodworth, C. Zhu, A. Mahan, Y. Ren, M. LaMorte, R. Gruber, A. Keane, P. Loring, L. Guo, T. H. Xia, B. Zhang, P. Orning, E. Lien, A. Degterev, T. Hammond, D. Ofengeim, RIPK1 activation mediates neuroinflammation and disease progression in multiple sclerosis. *Cell Rep.* 35, 109112 (2021).
- S. B. Kofman, L. H. Chu, J. M. Ames, S. D. Chavarria, K. Lichauco, B. P. Daniels, A. Oberst, RIPK3 coordinates RHIM domain-dependent antiviral inflammatory transcription in neurons. Sci. Signal. 18, eado9745 (2025).
- B. P. Daniels, S. B. Kofman, J. R. Smith, G. T. Norris, A. G. Snyder, J. P. Kolb, X. Gao, J. W. Locasale, J. Martinez, M. Gale Jr., Y. M. Loo, A. Oberst, The nucleotide sensor ZBP1 and kinase RIPK3 induce the enzyme IRG1 to promote an antiviral metabolic state in neurons. *Immunity* 50, 64–76.e4 (2019).
- B. P. Daniels, A. G. Snyder, T. M. Olsen, S. Orozco, T. H. Oguin III, S. W. G. Tait, J. Martinez, M. Gale Jr., Y. M. Loo, A. Oberst, RIPK3 restricts viral pathogenesis via cell death-independent neuroinflammation. *Cell* 169, 301–313.e11 (2017).
- M. Lindman, J. P. Angel, I. Estevez, N. P. Chang, T. W. Chou, M. McCourt, C. Atkins,
  B. P. Daniels, RIPK3 promotes brain region-specific interferon signaling and restriction of tick-borne flavivirus infection. *PLOS Pathog.* 19, e1011813 (2023).
- F. Giovannoni, F. J. Quintana, The role of astrocytes in CNS inflammation. *Trends Immunol.* 41. 805–819 (2020).
- K. Newton, D. L. Dugger, A. Maltzman, J. M. Greve, M. Hedehus, B. Martin-McNulty, R. A. Carano, T. C. Cao, N. van Bruggen, L. Bernstein, W. P. Lee, X. Wu, J. DeVoss, J. Zhang, S. Jeet, I. Peng, B. S. McKenzie, M. Roose-Girma, P. Caplazi, L. Diehl, J. D. Webster, D. Vucic, RIPK3 deficiency or catalytically inactive RIPK1 provides greater benefit than MLKL deficiency in mouse models of inflammation and tissue injury. *Cell Death Differ.* 23, 1565–1576 (2016)
- N. P. Chang, E. M. DaPrano, M. Lindman, I. Estevez, T. W. Chou, W. R. Evans, M. Nissenbaum, M. McCourt, D. Alzate, C. Atkins, A. W. Kusnecov, R. Huda, B. P. Daniels, Neuronal DAMPs exacerbate neurodegeneration via astrocytic RIPK3 signaling. *JCI Insight* 9, e177002 (2024).
- A. G. Snyder, N. W. Hubbard, M. N. Messmer, S. B. Kofman, C. E. Hagan, S. L. Orozco, K. Chiang, B. P. Daniels, D. Baker, A. Oberst, Intratumoral activation of the necroptotic pathway components RIPK1 and RIPK3 potentiates antitumor immunity. *Sci. Immunol.* 4, eaaw2004 (2019).
- C. Garber, A. Soung, L. L. Vollmer, M. Kanmogne, A. Last, J. Brown, R. S. Klein, T cells promote microglia-mediated synaptic elimination and cognitive dysfunction during recovery from neuropathogenic flaviviruses. *Nat. Neurosci.* 22, 1276–1288 (2019).
- M. A. Samuel, M. S. Diamond, Pathogenesis of West Nile Virus infection: A balance between virulence, innate and adaptive immunity, and viral evasion. *J. Virol.* 80, 9349–9360 (2006).
- M. C. Bouton, M. Geiger, W. P. Sheffield, J. A. Irving, D. A. Lomas, S. Song,
  R. S. Satyanarayanan, L. Zhang, G. McFadden, A. R. Lucas, The under-appreciated world of the serpin family of serine proteinase inhibitors. *EMBO Mol. Med.* 15, e17144 (2023).
- A. Sanchez-Navarro, I. Gonzalez-Soria, R. Caldino-Bohn, N. A. Bobadilla, An integrative view of serpins in health and disease: The contribution of SerpinA3. Am. J. Physiol. Cell Physiol. 320, C106–C118 (2021).
- T.-W. Chou, N. P. Chang, M. Krishnagiri, A. P. Patel, M. Lindman, J. P. Angel, P.-L. Kung,
  C. Atkins, B. P. Daniels, Fibrillar α-synuclein induces neurotoxic astrocyte activation via RIP kinase signaling and NF-κB. *Cell Death Dis.* 12, 756 (2021).
- M. Zhu, Z. Lan, J. Park, S. Gong, Y. Wang, F. Guo, Regulation of CNS pathology by Serpina3n/SERPINA3: The knowns and the puzzles. *Neuropathol. Appl. Neurobiol.* 50, e12980 (2024).
- N. Pastore, A. Ballabio, N. Brunetti-Pierri, Autophagy master regulator TFEB induces clearance of toxic SERPINA1/α-1-antitrypsin polymers. Autophagy 9, 1094–1096 (2013).
- K. Morgan, N. A. Kalsheker, Regulation of the serine proteinase inhibitor (SERPIN) gene alpha 1-antitrypsin: A paradigm for other SERPINs. *Int. J. Biochem. Cell Biol.* 29, 1501–1511 (1997).

- 44. A. Soman, S. Asha Nair, Unfolding the cascade of SERPINA3: Inflammation to cancer. *Biochim. Biophys. Acta Rev. Cancer* **1877**, 188760 (2022).
- K. Moriwaki, F. K. Chan, Necroptosis-independent signaling by the RIP kinases in inflammation. Cell. Mol. Life Sci. 73, 2325–2334 (2016).
- Y. Xu, F. Lin, G. Liao, J. Sun, W. Chen, L. Zhang, Ripks and neuroinflammation. *Mol. Neurobiol.* 61, 6771–6787 (2024).
- C. Wen, Y. Yu, C. Gao, X. Qi, C. J. Cardona, Z. Xing, RIPK3-dependent necroptosis is induced and restricts viral replication in human astrocytes infected with Zika virus. Front. Cell. Infect. Microbiol. 11. 637710 (2021).
- I. Estevez, B. D. Buckley, M. Lindman, N. Panzera, T. W. Chou, M. McCourt, B. J. Vaglio, C. Atkins, B. L. Firestein, B. P. Daniels, The kinase RIPK3 promotes neuronal survival by suppressing excitatory neurotransmission during central nervous system viral infection. *Immunity* 58, 666–682.e6 (2025).
- P. Wang, J. Dai, F. Bai, K. F. Kong, S. J. Wong, R. R. Montgomery, J. A. Madri, E. Fikrig, Matrix metalloproteinase 9 facilitates West Nile virus entry into the brain. J. Virol. 82, 8978–8985 (2008)
- A. Fortova, V. Honig, J. Salat, M. Palus, M. Pychova, L. Krbkova, A. V. Barkhash, M. F. Kriha,
  A. Chrdle, M. Lipoldova, D. Ruzek, Serum matrix metalloproteinase-9 (MMP-9) as a
  biomarker in paediatric and adult tick-borne encephalitis patients. Virus Res. 324, 199020 (2023).
- K. Roe, M. Kumar, S. Lum, B. Orillo, V. R. Nerurkar, S. Verma, West Nile virus-induced disruption of the blood-brain barrier in mice is characterized by the degradation of the junctional complex proteins and increase in multiple matrix metalloproteinases. *J. Gen. Virol.* 93, 1193–1203 (2012).
- M. J. Hannocks, X. Zhang, H. Gerwien, A. Chashchina, M. Burmeister, E. Korpos, J. Song, L. Sorokin, The gelatinases, MMP-2 and MMP-9, as fine tuners of neuroinflammatory processes. *Matrix Biol.* 75-76, 102–113 (2019).
- J. Song, C. Wu, E. Korpos, X. Zhang, S. M. Agrawal, Y. Wang, C. Faber, M. Schäfers, H. Körner, G. Opdenakker, R. Hallmann, L. Sorokin, Focal MMP-2 and MMP-9 activity at the blood-brain barrier promotes chemokine-induced leukocyte migration. *Cell Rep.* 10, 1040–1054 (2015).
- D. Acharya, P. Wang, A. M. Paul, J. Dai, D. Gate, J. E. Lowery, D. S. Stokic, A. A. Leis,
  R. A. Flavell, T. Town, E. Fikrig, F. Bai, Interleukin-17A promotes CD8<sup>+</sup>T cell cytotoxicity to facilitate West Nile virus clearance. *J. Virol.* 91, e01529-16 (2017).
- D. M. Durrant, M. L. Robinette, R. S. Klein, IL-1R1 is required for dendritic cell-mediated T cell reactivation within the CNS during West Nile virus encephalitis. J. Exp. Med. 210, 503–516 (2013).
- E. Gelpi, M. Preusser, U. Laggner, F. Garzuly, H. Holzmann, F. X. Heinz, H. Budka, Inflammatory response in human tick-borne encephalitis: Analysis of postmortem brain tissue. J. Neurovirol. 12, 322–327 (2006).
- H. L. Johnson, R. C. Willenbring, F. Jin, W. A. Manhart, S. J. LaFrance, I. Pirko, A. J. Johnson, Perforin competent CD8 T cells are sufficient to cause immune-mediated blood-brain barrier disruption. PLOS ONE 9, e111401 (2014).
- A. Aubert, M. Lane, K. Jung, D. J. Granville, Granzyme B as a therapeutic target: An update in 2022. Expert Opin. Ther. Targets 26, 979–993 (2022).
- G. Obasanmi, M. Uppal, J. Z. Cui, J. Xi, M. J. Ju, J. Song, E. To, S. Li, W. Khan, D. Cheng, J. Zhu, L. Irani, I. Samad, J. Zhu, H.-S. Yoo, A. Aubert, J. Stoddard, M. Neuringer, D. J. Granville, J. A. Matsubara, Granzyme B degrades extracellular matrix and promotes inflammation and choroidal neovascularization. *Angiogenesis* 27, 351–373 (2024).
- Y. Haile, K. C. Simmen, D. Pasichnyk, N. Touret, T. Simmen, J. Q. Lu, R. C. Bleackley,
  F. Giuliani, Granule-derived granzyme B mediates the vulnerability of human neurons to
  T cell-induced neurotoxicity. J. Immunol. 187, 4861–4872 (2011).
- F. Li, Y. Zhang, R. Li, Y. Li, S. Ding, J. Zhou, T. Huang, C. Chen, B. Lu, W. Yu, J. Boltze, P. Li, J. Wan, Neuronal Serpina3n is an endogenous protector against blood brain barrier damage following cerebral ischemic stroke. *J. Cereb. Blood Flow Metab.* 43, 241–257 (2023).
- Y. Zhang, Q. Chen, D. Chen, W. Zhao, H. Wang, M. Yang, Z. Xiang, H. Yuan, SerpinA3N attenuates ischemic stroke injury by reducing apoptosis and neuroinflammation. CNS Neurosci. Ther. 28, 566–579 (2022).
- Z.-M. Wang, C. Liu, Y.-Y. Wang, Y.-S. Deng, X.-C. He, H.-Z. Du, C.-M. Liu, Z.-Q. Teng, SerpinA3N deficiency deteriorates impairments of learning and memory in mice following hippocampal stab injury. *Cell Death Discov.* 6, 88 (2020).
- X. Ma, X. Niu, J. Zhao, Z. Deng, J. Li, X. Wu, B. Wang, M. Zhang, Y. Zhao, X. Guo, P. Sun, T. Huang, J. Wang, J. Song, Downregulation of Sepina3n aggravated blood-brain barrier disruption after traumatic brain injury by activating neutrophil elastase in mice. *Neuroscience* 503, 45–57 (2022).
- Y. Haile, K. Carmine-Simmen, C. Olechowski, B. Kerr, R. C. Bleackley, F. Giuliani, Granzyme B-inhibitor serpina3n induces neuroprotection in vitro and in vivo. J. Neuroinflammation 12, 157 (2015)
- L. Vicuna, D. E. Strochlic, A. Latremoliere, K. K. Bali, M. Simonetti, D. Husainie, S. Prokosch,
  P. Riva, R. S. Griffin, C. Njoo, S. Gehrig, M. A. Mall, B. Arnold, M. Devor, C. J. Woolf,
  S. D. Liberles, M. Costigan, R. Kuner, The serine protease inhibitor SerpinA3N attenuates

#### SCIENCE SIGNALING | RESEARCH ARTICLE

- neuropathic pain by inhibiting T cell-derived leukocyte elastase. *Nat. Med.* **21**, 518–523 (2015).
- 67. H. Kim, K. Leng, J. Park, A. G. Sorets, S. Kim, A. Shostak, R. J. Embalabala, K. Mlouk, K. A. Katdare, I. V. L. Rose, S. M. Sturgeon, E. H. Neal, Y. Ao, S. Wang, M. V. Sofroniew, J. M. Brunger, D. G. McMahon, M. S. Schrag, M. Kampmann, E. S. Lippmann, Reactive astrocytes transduce inflammation in a blood-brain barrier model through a TNF-STAT3 signaling axis and secretion of alpha 1-antichymotrypsin. *Nat. Commun.* 13, 6581 (2022).
- C. Liu, X. M. Zhao, Q. Wang, T. T. Du, M. X. Zhang, H. Z. Wang, R. P. Li, K. Liang, Y. Gao, S. Y. Zhou, T. Xue, J. G. Zhang, C. L. Han, L. Shi, L. W. Zhang, F. G. Meng, Astrocyte-derived SerpinA3N promotes neuroinflammation and epileptic seizures by activating the NF-κB signaling pathway in mice with temporal lobe epilepsy. *J. Neuroinflammation* 20, 161 (2023).
- X. Han, Q. Lei, H. Liu, T. Zhang, X. Gou, SerpinA3N regulates the secretory phenotype of mouse senescent astrocytes contributing to neurodegeneration. J. Gerontol. A Biol. Sci. Med. Sci. 79, glad 278 (2024).
- M. Zattoni, M. Mearelli, S. Vanni, A. Colini Baldeschi, T. H. Tran, C. Ferracin, M. Catania, F. Moda, G. Di Fede, G. Giaccone, F. Tagliavini, G. Zanusso, J. W. Ironside, I. Ferrer, G. Legname, Serpin signatures in prion and Alzheimer's diseases. *Mol. Neurobiol.* 59, 3778–3799 (2022).
- M. Santamaria, A. Pardo-Saganta, L. Alvarez-Asiain, M. Di Scala, C. Qian, J. Prieto,
  M. A. Avila, Nuclear α1-antichymotrypsin promotes chromatin condensation and inhibits proliferation of human hepatocellular carcinoma cells. *Gastroenterology* 144, 818–828.e4 (2013)
- A. G. Almonte, J. D. Sweatt, Serine proteases, serine protease inhibitors, and proteaseactivated receptors: Roles in synaptic function and behavior. Brain Res. 1407, 107–122 (2011).
- G. Wiera, J. W. Mozrzymas, Extracellular proteolysis in structural and functional plasticity of mossy fiber synapses in hippocampus. Front. Cell. Neurosci. 9, 427 (2015).
- T.W. Lee, V. W. Tsang, N. P. Birch, Physiological and pathological roles of tissue plasminogen activator and its inhibitor neuroserpin in the nervous system. Front. Cell. Neurosci. 9, 396 (2015).
- M. Ferrer-Ferrer, S. Jia, R. Kaushik, J. Schneeberg, I. Figiel, S. Aleshin, A. Mironov, M. Safari, R. Frischknecht, J. Wlodarczyk, O. Senkov, A. Dityatev, Mice deficient in synaptic protease neurotrypsin show impaired spaced long-term potentiation and blunted learninginduced modulation of dendritic spines. *Cell. Mol. Life Sci.* 80, 82 (2023).
- A. Canciani, C. Capitanio, S. Stanga, S. Faravelli, L. Scietti, L. Mapelli, T. Soda, E. D'Angelo, P. Kienlen-Campard, F. Forneris, Deconstruction of neurotrypsin reveals a multi-factorially regulated activity affecting myotube formation and neuronal excitability. *Mol. Neurobiol.* 59, 7466–7485 (2022).
- A. Elong Ngono, T. Syed, A. V. Nguyen, J. A. Regla-Nava, M. Susantono, D. Spasova,
  A. Aguilar, M. West, J. Sparks, A. Gonzalez, E. Branche, J. L. DeHart, J. B. Vega, P. P. Karmali,

- P. Chivukula, K. Kamrud, P. Aliahmad, N. Wang, S. Shresta, CD8<sup>+</sup>T cells mediate protection against Zika virus induced by an NS3-based vaccine. *Sci. Adv.* **6**, eabb2154 (2020).
- J. D. Brien, J. L. Uhrlaub, J. Nikolich-Zugich, Protective capacity and epitope specificity of CD8<sup>+</sup>T cells responding to lethal West Nile virus infection. *Eur. J. Immunol.* 37, 1855–1863 (2007).
- J. Netland, M. J. Bevan, CD8 and CD4T cells in West Nile virus immunity and pathogenesis. Viruses 5, 2573–2584 (2013).
- E. E. McCandless, B. Zhang, M. S. Diamond, R. S. Klein, CXCR4 antagonism increases T cell trafficking in the central nervous system and improves survival from West Nile virus encephalitis. *Proc. Natl. Acad. Sci. U.S.A.* 105, 11270–11275 (2008).
- J. M. Murphy, P. E. Czabotar, J. M. Hildebrand, I. S. Lucet, J. G. Zhang, S. Alvarez-Diaz, R. Lewis, N. Lalaoui, D. Metcalf, A. I. Webb, S. N. Young, L. N. Varghese, G. M. Tannahill, E. C. Hatchell, I. J. Majewski, T. Okamoto, R. C. Dobson, D. J. Hilton, J. J. Babon, N. A. Nicola, A. Strasser, J. Silke, W. S. Alexander, The pseudokinase MLKL mediates necroptosis via a molecular switch mechanism. *Immunity* 39, 443–453 (2013).
- 82. F. J. May, L. Li, C. T. Davis, S. E. Galbraith, A. D. T. Barrett, Multiple pathways to the attenuation of West Nile virus in south-east Texas in 2003. *Virology* **405**, 8–14 (2010).
- P.-L. Kung, T.-W. Chou, M. Lindman, N. P. Chang, I. Estevez, B. D. Buckley, C. Atkins,
  B. P. Daniels, Zika virus-induced TNF-α signaling dysregulates expression of neurologic genes associated with psychiatric disorders. *J. Neuroinflammation* 19, 100 (2022).

Acknowledgments: We thank Z. Tanvir of the Rutgers SAS-HGINJ Imaging Core Facility for assistance with confocal microscopy. We thank A. Oberst (University of Washington), B. Herrera (Robert Wood Johnson Medical School), and Genentech Inc. for the provision of key reagents and transgenic animals. Funding: This work was supported by R01 NS120895 (to B.P.D.) and R00 HD103911 (to N.M.O.). I.E. was supported by a Howard Hughes Medical Institute Gilliam Fellowship. Author contributions: Conceptualization: M.L. and B.P.D. Investigation: M.L., I.E., E.M., K.N., C.A., N.M.O., and B.P.D. Analysis: M.L., I.E., E.M., E.M.D., T.-W.C., N.M.O., and B.P.D. Resources: N.M.O. and B.P.D. Writing—original draft: M.L., E.M., and B.P.D. Writing—review and editing: M.L., C.A., N.M.O., and B.P.D. Supervision: C.A., N.M.O., and B.P.D. Funding acquisition: N.M.O. and B.P.D. Competing interests: The authors declare that they have no competing interests. Data and materials availability: RNA-seq data generated in this study are deposited in NCBI's Gene Expression Omnibus and can be accessed under accession number GSE268520. All other data needed to evaluate the conclusions in the paper are present in the paper or the Supplementary Materials.

Submitted 23 May 2024 Accepted 25 June 2025 Published 15 July 2025 10.1126/scisignal.adq6422